

# Sidechain Dynamics and Protein Folding

Edo Kussell<sup>1</sup>, Jun Shimada<sup>2</sup>, Eugene I. Shakhnovich<sup>2\*</sup>

October 28, 2018

**Running title:** Sidechain Dynamics

48 pages (including figure/table captions), 13 figures, 3 tables.

**manuscript:** “sc dynamics.tex” (LaTeX document)

<sup>1</sup>Department of Biophysics  
Harvard University  
240 Longwood Ave.  
Boston, MA 02115

<sup>2</sup>Department of Chemistry and Chemical Biology  
Harvard University  
12 Oxford Street  
Cambridge MA 02138

\*corresponding author

tel: 617-495-4130

fax: 617-496-5948

email: eugene@belok.harvard.edu

## **Abstract**

The processes by which protein sidechains reach equilibrium during a folding reaction are investigated using both lattice and all-atom simulations. We find that rates of sidechain relaxation exhibit a distribution over the protein structure, with the fastest relaxing sidechains being involved in kinetically important positions. Traversal of the major folding transition state corresponds to the freezing of a small number of residues, while the rest of the chain proceeds towards equilibrium via backbone fluctuations around the native fold. The post-nucleation processes by which sidechains relax are characterized by very slow dynamics, and many barrier crossings, and thus resemble the behavior of a glass. At optimal temperature, however, the nucleated ensemble is energetically very close to equilibrium; slow relaxation is still observed. At lower temperatures, sidechain relaxation becomes a significant and very noticeable part of the folding reaction.

**Keywords:** sidechain dynamics, protein folding, nucleation mechanism, glass transition, sidechain packing

# Introduction

Protein folding is a complex, single molecule process in which a polypeptide backbone with diverse sidechain groups efficiently searches a vast conformational space and finds a unique native fold. Most theoretical attempts to understand the folding process have modeled the polymer, in one way or another, as a chain of beads which undergoes a backbone freezing transition. The internal degrees of freedom of each sidechain (the  $\chi$  angles) add another layer of difficulty to understanding the folding process.

In unfolded conformations, the barriers between rotamer states of sidechains are low<sup>1</sup> and sidechains easily convert between them. Upon folding, buried sidechains are usually found in a single, well-defined rotamer state,<sup>2-5</sup> and interconversion between rotamers, when energetically allowed, is slow due to high barriers.<sup>6,7</sup> Because protein folding is thought to be a sidechain-driven process, finding the native rotamers is an integral part of the folding reaction. Do sidechains reach their native conformations simultaneously with the backbone, or is sidechain ordering a separate process that occurs after the native fold has been reached? This question poses a challenge for experimentalists and theoreticians alike.

We study the dynamics of sidechains during the folding process via a simplified model, which captures the basic physical aspects of the problem, as well as an all-atom protein folding simulation, in which the full complexity of sidechain shapes and mobility is represented. We start by modifying the classic lattice model of proteins to account for internal sidechain states of each amino-acid. This new model, like its predecessors, is found to fold in a cooperative all-or-none manner. The presence of internal degrees of freedom at each site, however, allows the backbone to reach the native conformation before all of the sidechains have become properly ordered. Since energy comes

from sidechain-sidechain interactions, completion of the folding reaction requires both the backbone and the sidechains to reach their native states. We find that, depending on simulation temperature, the backbone can become native-like long before the internal sidechain states reach equilibrium. By measuring the rate of sidechain ordering for each monomer, we find that there is a cluster of residues whose sidechains become ordered very fast, while the relaxation rates of other positions is up to an order of magnitude slower. The fast cluster turns out to be very close to the folding nucleus identified previously for the structure we use.

A small number of kinetically important residues thus freeze in their native “rotamer” state on a fast timescale, pulling the backbone strongly toward its native conformation, while the rest of the protein relaxes on a slower timescale toward its equilibrium energy. This slow phase could not be observed in previous lattice simulations because it arises entirely from the presence of the internal sidechain states of each monomer. We find that the slow-phase relaxation of energy to equilibrium follows stretched-exponential kinetics, suggesting that the dynamics are exhibiting some glass-like properties due to sidechains. We note that backbone-only lattice models have been shown to be free of a glass transition over a wide range of temperatures.<sup>8</sup> Various experimental and theoretical studies have suggested that some aspects of protein folding might be interpreted as glassy behavior,<sup>9–12</sup> though whether these phenomena are attributable to backbone, sidechains, or solvent remains to be seen.

Because the lattice model is computationally very fast, one can observe relaxation to equilibrium even at lower temperatures. This becomes impossible once more realistic models are used. Our previous work using an all-atom simulation, with a simplified Gō potential,<sup>13</sup> demonstrated that folding to the native backbone topology (rms deviation  $< 1$  Å from crystal structure) happened within a reasonable amount of time, but that full relaxation to equilibrium could not be observed at

temperatures below a certain threshold. Thus the slow phase observed in the lattice model is also present in the all-atom model, but cannot be fully characterized therein due to prohibitively long simulation times. This does not prevent us from identifying the residues that exhibit fast transition to the native state, because the fast phase in which the native backbone conformation is reached is fully accessible to our simulation. We characterize the folding transition state of Protein G using the all-atom simulation. We also identify the residues whose sidechains exhibit fast relaxation to their native state. We find that these same residues play a key role in the transition state ensemble. As in the simpler lattice model, we find a wide distribution of sidechain relaxation times. Two very different models are thus in marked agreement; together they provide a clear picture of sidechain dynamics during the folding process.

## Results

In order to mimic the internal degrees of freedom of protein sidechains (the  $\chi$  angles), we modified the standard lattice model by adding  $n$  sidechain states to each residue. This is consistent with the observation that protein sidechains usually populate discrete rotameric configurations.<sup>2,3</sup> The state of each residue at any given time is a number between 0 and  $n - 1$ . Of these  $n$  states only one state (the 0 state) was designated as native for each residue. When two residues came into contact during simulation, they interacted only if both were in their native state - a contact formed with one or both residues in a non-native sidechain state did not contribute to the energy of the conformation (see Methods). While there are other ways to model a native vs. non-native rotamer interaction using a lattice model (for example, we could have assigned some fraction of the native energy when non-native monomers interact), we chose the present scheme for simplicity. Previous lattice models

have added sidechain degrees of freedom by letting sidechains occupy a lattice site.<sup>14-16</sup> In our model, sidechain states are treated implicitly, resulting in a considerable computational advantage.

An important aspect of sidechain motion in real proteins is that upon compactification of the polypeptide chain, sidechain motion is restricted due to the excluded volume effect.<sup>1,17</sup> In order for sidechains to repack in the protein interior, the backbone must perform a “breathing motion”,<sup>6</sup> allowing sidechains some extra room to move, and thus making certain sidechain configurations momentarily available. Any model of sidechain dynamics must incorporate this effect in some way. Our all-atom simulation contains this effect explicitly. In the lattice simulation we mimic this effect by our choice of moves. In addition to the usual lattice backbone moves, we allow the sidechain states of a given residue to interconvert when there are no other residues in contact with it (see Methods). Thus, when the chain is fully compact, the sidechain states are frozen until a backbone fluctuation frees some residues, and allows their states to change.

We tested the lattice model with 1, 2, 4, and 8 internal states per monomer using a 27-mer sequence designed to fold into a 3 x 3 x 3 cube. The  $n = 1$  model corresponds to the standard lattice model and is shown here only as a control. The thermodynamics of these four models is shown in Figure 1A. All are seen to exhibit a cooperative temperature transition, with the transition temperature getting progressively lower as the number of internal states of each monomer increases. The lowered transition temperature is to be expected as the increased entropy of the model (due to more internal states) necessarily leads to some destabilization. The transition region becomes narrower as  $n$  increases, due to the increase in entropy of the unfolded state relative to the folded state.

We studied the kinetics of the various models by plotting the average folding time as a function of temperature (see Figure 2, panels A, B, and C). The models with  $n > 1$  possess the property

that the backbone can reach full nativity before all of the sidechains have become native. This leads to the interesting question of how the polymer chain reaches its native energy. That is, does the formation of the native backbone lead to immediate sidechain ordering, or do sidechains relax slowly to equilibrium after the chain has folded?

To answer this question, we plotted both the average time to reach the native energy (which corresponds to full sidechain ordering), and the average time to reach the native backbone in Figure 2. We find that at temperatures above the optimal folding temperature, the native energy is reached immediately after the native backbone is found, and thus sidechain ordering is fast. At low temperatures, on the other hand, the native backbone is reached long before native energy is achieved, and sidechain ordering is slow. The shift between these two behaviors appears to be continuous in temperature, but depends on the number of sidechain states,  $n$ , per residue. For the  $n = 2$  model (panel A), the shift from fast to slow sidechain ordering occurs at the relatively low temperature of 12.5 which is about 60% of the temperature of fastest folding,  $T_{opt}$ . For the  $n = 4$  model (panel B), we see that the delay between backbone folding and full ordering is noticeable even at  $T_{opt}$ , and becomes significant at  $T = 13.3$  which is 85% of  $T_{opt}$ . The same is observed for the  $n = 8$  model (panel C). Thus the increase in sidechain entropy of the chain leads to a severe sidechain-ordering trap. This trap becomes increasingly prominent as the entropy of the model increases, and the temperature at which it becomes noticeable moves closer and closer to  $T_{opt}$ .

The mechanism for reaching full nativity (backbone and sidechains) at temperatures lower than  $T_{opt}$  thus seems to be one in which the native backbone structure is formed, followed by sidechain ordering via backbone fluctuations around the native structure. It is entirely possible, however, that the native backbone structure is reached during the folding trajectory but unfolds immediately because too few sidechains are native. This, in fact, is the case even at low temperatures. At some

point in time, however, the native backbone structure is reached with enough native sidechains to remain stable long enough to allow the rest of the sidechains to become ordered. It is the ordering of sidechains after this *stable* native backbone is reached that we identify as an important kinetic step at temperatures below  $T_{opt}$ . Accordingly, we plot the average time of the *last* pass to the native backbone conformation in all of our figures. The time of the last pass is defined as the first time the chain reached the native backbone without losing more than 50% of its native contacts before reaching the native energy. We found that our results did not change significantly when we varied the fraction of native contacts used in this definition.

It is instructive to obtain a kinetic picture for an “unhindered” model in which the sidechain states of each residue can interconvert freely, regardless of its surroundings. Such a model represents protein folding in molten globule conditions, in which sidechain rotamers can easily interconvert. We see in Figure 2D that in the unhindered model, the slow ordering of sidechains is not observed at any temperature. Instead, once the backbone reaches nativity, any non-native sidechains can immediately become native, and they do because it is energetically favorable. This control demonstrates, then, that the sidechain ordering trap is a feature of folding under conditions in which a tight native state, with low sidechain mobility, is the free-energy minimum.

We compare the kinetics of the unhindered model with  $n = 2$  with the kinetics of the standard lattice model ( $n = 1$ ). We find that at their respective optimal folding temperatures, the average time to reach the native energy for both models is the same (Figure 2D). The freely interconverting internal states, then, do not have any effect on the kinetics of folding; they only affect the stability of the model. On the other hand, the folding time of the hindered models with  $n > 1$  at  $T_{opt}$  is significantly slower than that of the 1-state model. This makes sense in light of the observation that the hindered models are more difficult to nucleate, for the following reason: if a proper nucleus



forms and one or more of its sidechains are in a non-native state, the nucleus will almost certainly break apart because the energy of each of its contacts is crucial for its ability to function as a nucleus.<sup>18</sup> The sidechains cannot interconvert while the nucleus contacts are present, and therefore the nucleus dissolves. In the unhindered model, the non-native sidechain states of a nucleus can become native with the nucleus intact, so the folding time in this model is not affected by the presence of sidechain states.

Having observed that folding to the correct backbone structure occurs significantly before the native energy is reached, we asked the following questions: Do some residues reach their native sidechain state faster than others? If so which ones are fast, which ones are slow, and why? We decided to study a 48-mer structure whose folding in the standard lattice model has been studied exhaustively.<sup>19</sup> In order to maximize the temperature range in which we could study folding of this structure, we used a sequence that has been optimized for fast folding.<sup>20</sup> In addition to having a fully characterized nucleus, using a 48-mer sequence allowed us to see whether our results were sensitive to the size of the structure.

The thermodynamics of the 48-mer sequence are shown in Figure 1B. The kinetics for the 4-state model are shown in Figure 3. We consider a kinetic model with three steps:



Figure 3B shows the average time of the first and second steps plotted as diamonds and crosses, respectively. We immediately see that for high temperatures, the sidechain ordering step is several orders of magnitude faster than the backbone folding step. As temperature becomes lower, the sidechain ordering time becomes comparable to the backbone folding time. At  $T = 0.13 = 85\% T_{opt}$ , the rate of sidechain ordering becomes significant as it comes within an order of magnitude of the rate of backbone folding. The 48-mer sequence in the 4-state model, then, is seen to behave very

much like the 27-mer 4-state model, with both models developing a significant sidechain ordering step in kinetics at 85% of  $T_{opt}$ .

In order to obtain individual sidechain ordering rates for each residue, we performed many long folding runs. For each residue we averaged its sidechain state over all folding runs: we assigned a value of 1 to the native internal state of a given residue, and a value of 0 to all other internal states, and at each timestep averaged these values over runs. Two traces obtained after averaging are shown in Figure 4. We fit a single exponential (see Methods) to each trace, and obtained time constants for each of the 48 residues.

The distribution of rate constants for two temperatures is given in Figure 5, and the fast residues are labelled by number. The first striking feature is that these distributions span two orders of magnitude. At the lower of the two temperatures ( $T = 7.4 = 81\% T_{opt}$ ), most residues exhibit slow relaxation rates, as seen by the sharp peak near zero. At the higher temperature of  $T_{opt} = 9.1$ , the height of the peak is reduced and more residues are seen with faster rates.

At both temperatures, a small number of residues have very fast rates. Many of these fast residues belong to the folding nucleus for this structure that was identified in another study<sup>19,20</sup> using the standard lattice model. In Figure 6 we show the 48-mer structure colored by rate of sidechain freezing at  $T = 7.4$ , and we indicate the original nucleus by large spheres. Of the 10 fastest residues that become fully ordered at  $T = 7.4$ , 7 belong to the folding nucleus. While some of the nucleus positions are no longer kinetically important in the present model, a strong signature of the old nucleus has remained. Importantly, with the exception of residue 9, all of the fast positions that reach full nativity are located in or near the original nucleus was found.

It appears, then, that at temperatures at or below  $T_{opt}$ , a small group of residues reaches full nativity quickly, thus organizing a critical piece of structure which remains fully stable, allowing

the rest of the chain to gradually order its sidechains. At  $T = 7.4$ , the formation of the stable piece traps many sidechains in non-native states which take a very long time to reorganize via backbone fluctuations. On the other hand, at  $T_{opt}$ , as seen in Figure 5, more residues are found in the fast tail of the rate distribution, indicating that backbone fluctuations are sufficient to allow sidechain ordering to occur more quickly once enough native structure has formed. Additionally, the higher temperature requires a larger amount of native structure to be formed in order to remain stable. These two effects act to eliminate sidechain ordering as a relevant kinetic step at  $T_{opt}$ . This is seen clearly in Figure 3 where at  $T_{opt}$  the sidechain ordering step is an order of magnitude faster than the backbone folding step.

Another way to see that sidechain dynamics becomes markedly different as temperature is lowered is given in Figure 7. The red line indicates the equilibrium energy at each of the two temperatures, while the solid green line is a time trace of the average energy over all runs. The average time to form the stable native backbone is  $2.7 \times 10^7$  at  $T = T_{opt} = 9.1$ , and  $1.6 \times 10^8$  at  $T = 7.4$ , and is marked by an arrow in the figure. For  $T = T_{opt}$ , the arrow indicates that at the time of native backbone formation, the energy of the chain is already very close to its equilibrium value. That is not the case at low temperature, at which there is a significant gap between the energy of the folded chain and the equilibrium energy.

We tried to fit the relaxation of energy by a standard, single-barrier process (single exponential) as well as a double exponential fit - both fits converged to the same curve which is shown as a dashed line in Figure 7. The fit is not appropriate at any timescale. In particular, we note that at short times, the trajectory may resemble a single-exponential process, but it develops a very long tail at long times. We fit the long tail using a stretched exponential,  $b_1 \exp(-b_2 t^\alpha)$ , and found  $\alpha = 0.09$ ; the relaxation is therefore practically logarithmic at long times (see Figure 7 caption for details).

At short times we fit a single-exponential. These fits were done at  $T = 9.1$  and are shown as the solid black line in Figure 7. At  $T = 7.4$  we did not have enough data at long times to see relaxation to equilibrium and therefore a fit would not be meaningful. The fit of energy relaxation using a single-exponential at short times, and a stretched exponential at long times is very good. The single-exponential phase corresponds to the classic nucleation mechanism in which the backbone topology becomes organized.<sup>18</sup> The stretched exponential phase is a signature of glassy dynamics associated with the sidechain degrees of freedom and will be discussed below.

Because lattice models can give only a schematic view of the folding process, we proceeded to investigate sidechain dynamics in an all-atom simulation of Protein G, an alpha/beta protein that has featured in numerous experiments.<sup>21-23</sup> The details of the simulation and a full characterization of the folding kinetics of this protein will be given elsewhere. Our goal in the present study is to see how the results obtained from our simplified lattice model compare with a much more realistic representation of a protein, and whether the same kind of analysis can shed light on the kinetics of a real protein. In the lattice model we had to postulate a set of microscopic dynamics for the internal states of each residue. In the all-atom simulation, we model all sidechain atoms and torsions explicitly. We use the simulation methodology described previously.<sup>24</sup> Because rotations around sidechain  $\chi$  angles are continuous, interconversion between sidechain rotamers can become restricted if a residue is buried. Slowing down of sidechain dynamics upon compactification emerges from the excluded volume interaction in this model, and does not have to be included phenomenologically as in the lattice model.

We obtained 50 folding trajectories of Protein G, starting from random backbone and sidechain conformations, all at the same temperature. All runs were terminated after  $2 \times 10^9$  steps, by which time 47 had reached the native backbone fold (see Methods). We then applied a time series analysis

similar to the one we used for the lattice model. Specifically, at each time step and for each residue we recorded a value of 1 if the sidechain was in its native rotameric state, and a 0 otherwise. We averaged these values for each residue over all trajectories, and then fit a kinetic model to the resulting traces. The parameters for the fits for each residue are given in Tables 2 and 3.

Protein G folds in simulations via a kinetic intermediate consisting of either hairpin 1 and the helix or hairpin 2 and the helix (see Discussion). A two-state fit was therefore not appropriate for some of the residues. We used a three-state fit for all residues, and found that for some of the residues one rate constant was at least an order of magnitude larger than the other. Such residues were classified as two-state, while the others were classified as three-state. Figure 8 shows representative fits for two-state and three-state residues. The relaxation rates given in Tables 2 and 3 span an order of magnitude. The equilibrium level of ordering of each residue (parameter  $d$  in the Tables) was obtained directly as an average over a long simulation started in the native state, and was not obtained by fitting. Some residues are seen to be highly ordered in the native state, while others are not. We looked at the fastest residues whose equilibrium level was at least 70% ordered (bold residues in the Tables).

The four fastest two-state residues are shown in Figure 9. These four make key contacts between the first hairpin and the helix. Phenylalanine 30 and leucine 5 have a strong hydrophobic interaction that secures the first strand of the hairpin against the helix, while threonines 18 and 25 lock in the second beta strand. The fastest two-state residues are thus seen to be important in forming the kinetic intermediate. All residues involved in intermediate formation are naturally found to be two-state, because formation of the intermediate is a purely two-state process.

The three-state residues are ones whose sidechain ordering cannot proceed normally until the intermediate has formed. They exhibit a lag phase as seen in Figure 8 while the intermediate forms.

In Figure 10 we show the three fastest three-state residues of Protein G which are significantly ordered at equilibrium: valines 6 and 54 and phenylalanine 52. Interestingly, these three residues all have the same rate of relaxation, suggesting that they become ordered together. All three are involved in bringing beta-strand 4 in hairpin 2 into contact with the rest of the protein. Valine 6 establishes contacts between beta-strands 1 and 4. Valine 54 makes contacts with valine 39 (located at the C-terminus of the helix) which hold the end of hairpin 2 against the helix. Phenylalanine 52 makes hydrophobic contacts with tyrosine 45, stabilizing hairpin 2 internally, while also making contacts with the helix.

The data obtained from the all-atom simulation is in good qualitative agreement with our lattice simulation. There is a wide distribution of residue relaxation rates, with the fast residues located in topologically important positions. The same mechanism seems to be at work here: key organizing residues form quickly holding the overall structure together, while all other residues relax more slowly toward equilibrium via fluctuations around the native fold. On the lattice we found strong overlap between the fast residues and the nucleus residues which organized the backbone transition state. In order to make a similar comparison in the all-atom model, we proceeded to characterize its transition state ensemble.

Because the transition state ensemble lies at the top of the folding free energy landscape, its conformations are characterized by a 0.5 probability of folding ( $p_{\text{fold}}$ ) during a tiny fraction of the entire folding time (“commitment time”<sup>25</sup>). Assuming a commitment time corresponding to 0.005% of a full folding run, we calculated the  $p_{\text{fold}}$  of approximately 5 structures per trajectory. A histogram of contacts (Figure 11) made by each residue for various  $p_{\text{fold}}$  ensembles reveals that phenylalanine 52 is the most important residue for the final intermediate  $\rightarrow$  native folding step. Its energy contribution, which is proportional to the number of contacts it makes, appears to grow as

the ensemble  $p_{\text{fold}}$  approaches one. Though less pronounced, similar increases were seen for Y3, K4, L5, V6, A23, E27, F30, W43, Y45, K50, and V54. When individual residue-residue contacts are histogrammed (Figure 12), it is clear that only a handful of over 1500 possible contacts are important for stabilizing the transition state ensemble. These special contacts bring two hairpin 2 residues (F52 and V54) in contact with hairpin 1 (Y3, L5, V6) and helix residues (E27 and F30). Because of the non-local and specific nature of these contacts, folding in this model appears to be consistent with that proposed under the theory of specific nucleation.<sup>18,26-29</sup> Detailed comparison of these results with experimental data will be presented elsewhere (JS, EIS, manuscript in preparation).

It is clear that the nucleus characterizing the transition state ensemble under our all-atom model of folding is nicely identified by the time-series analysis of sidechain dynamics. The three fastest three-state residues - V6, F52, and V54 - coincide with those which are most indicative of progress along the  $p_{\text{fold}}$  hypersurface. Although structures with  $p_{\text{fold}} \approx 1$  will rapidly attain native-like backbone topologies, energies will reach equilibrium values very slowly, requiring simulations extending beyond the  $2 \times 10^9$  cutoff we have used here. This is because a fairly significant amount of energy is contributed by sidechain-sidechain interactions, and the correct packing of sidechains is significantly slower once the collapse transition has occurred. In our previous study of crambin, we observed a similar phenomenon (which we referred to as the “sidechain-packing trap”; see Figure 6E in reference<sup>24</sup>), where the folding of the backbone occurred on a faster timescale than that by which the native energy was fully attained. The current  $p_{\text{fold}}$  analysis demonstrates that, in fact, not all residues participate equally in the slow relaxation of conformations with incorrect packing. The nucleus residues (V6, F52, V54) have to attain native packing relatively early as their energy contribution is required to counterbalance the tremendous loss of backbone entropy upon collapse to a native-like conformation.

Finally, we also note a striking similarity between the thermodynamic data of the lattice model presented here and crambin obtained from all-atom simulations. For crambin, we observed a rather unusual departure from a simple two state model when fitting the equilibrium energy against temperature. As temperature was lowered below the transition point, the decrease in energy was perfectly linear with temperature. As shown in Figure 1 (particularly for the 48-mer), as the number of sidechain states is increased, the same linear relation between energy and temperature is observed. This suggests that sidechain degrees of freedom lead to a noticeable contribution to the heat capacity, which dominates the thermodynamic behavior at low temperatures.

## Discussion

Extracting information about the dynamics of individual sidechains is relatively easy in computational studies and veritably challenging in experiments. There are several difficulties to overcome in experiments. First, specific probes that measure properties about a single residue are scarce: tryptophan can be probed by fluorescence, while cysteine can be probed by thiol-disulfide exchange. While dynamic NMR techniques can in principle report on many residues simultaneously, their application requires very slow folding reactions. Hydrogen exchange experiments<sup>30</sup> can report on the protection of individual backbone amide groups, but backbone protection factors do not directly measure sidechain mobility. Second, it is desirable to have probes in several different parts of a structure in order to measure the distribution of sidechain rate constants over the whole fold. This, again, is in principle possible but usually requires introducing sequence mutations (adding a tryptophan or cysteine). Results must therefore be handled with care because the structure and folding pathways may be altered in subtle ways from sequence to sequence. Finally, the presence of



kinetic intermediates in the folding of many proteins complicates analysis considerably.

Several recent studies have attacked the sidechain dynamics question using a variety of techniques. Staniforth and coworkers<sup>31</sup> used a form of cystatin in which disulfide bonds were reduced, thus creating a molten globule whose compactness and unfolding properties were similar to folded wild type, but whose sidechain mobility was significantly increased. The size of the rate-limiting barrier for folding of the two forms was measured and found to be similar. The authors conclude that since the reduced and wild type forms differ mainly in sidechain mobility, while the barrier height for folding is the same, the immobilization of sidechains occurs after the major folding transition in wild type cystatin. Additional experiments on cystatin are probably needed in order to completely solidify the argument. Specifically, the connection between fluorescence quenching upon folding and full sidechain immobilization in wild type cystatin has not been made; thus, any conclusions about sidechain immobilization rest on the assumption that nativity of tryptophan fluorescence gives information about sidechain dynamics across the entire core.

Ha and Loh<sup>32</sup> introduced cysteine mutations in several key places in apomyoglobin and, using pulsed thiol-disulfide exchange at different times during the folding reaction, measured the progression of side chain ordering at each site. They found that certain locations, stabilizing the fast-forming folding intermediate, were as well-packed as native protein long before folding was complete. It would be interesting to obtain similar site-specific time courses for other positions distributed across the protein and to see whether positions that become ordered in the post-intermediate step exhibit a distribution of relaxation times.

In an elegant series of experiments using time-resolved fluorescence anisotropy measurements, Sridevi and coworkers<sup>33</sup> demonstrated that barstar's tryptophan 53 becomes fully ordered approximately 8 times faster than the rate of the slow folding reaction of the protein. By observing

fluorescence lifetime decay, they could watch the initially evenly populated rotamers of tryptophan reach nativity in which one rotamer is 88% populated. The authors suggest that rapid relaxation of tryptophan indicates the existence of an intermediate during the slow folding of barstar. It is not clear, however, that this must be the case. An alternate explanation is that there exists a significant spread among sidechain relaxation rates within a single folding reaction.

Our work demonstrates that the presence of sidechain degrees of freedom leads to a wide distribution of residue relaxation rates, even within two-state cooperative folding reactions. Figure 13 gives a schematic overview of the relaxation mechanism we observed. Both in lattice and in all-atom simulations, we found a small number of residues becoming fully ordered much faster than the rest of the protein. This observation is consistent with the nucleation-condensation view of protein folding in which the major transition state of the folding reaction involves a few residues reaching their native conformation. Importantly, in our simulations, we find that these nucleating residues are not only in correct spatial geometry with respect to each other's centers of mass, but additionally their native rotamer has been singled out and practically frozen. Once nucleation has occurred, the native chain topology is strongly stabilized and certain measures, such as compactness and perhaps fluorescence, might indicate that the reaction is complete, and equilibrium has been reached (see Figure 13 after nucleation barrier). This, however, is not the case as there exist many sidechains that have become partially ordered, yet have still not reached equilibrium. Because the nucleating residues have frozen and are rigid, and many other partially ordered residues are significantly stabilizing the fold, the non-equilibrated sidechains are not able to convert easily to their native rotamer. They remain in a non-native state until a backbone fluctuation momentarily allows them to interconvert. The presence of backbone breathing motions in protein globules may therefore be useful not only for function, as has been suggested before,<sup>34,35</sup> but also in order to allow sidechain

equilibrium to be achieved in a reasonable amount of time.

In simulations, a kinetic intermediate is very easily observed as a set of conformations which appears as a plateau within some range of energies during many folding trajectories.<sup>24,36</sup> In the Protein G simulations, the major folding pathway consisted of formation of hairpin 1 and the helix followed by formation of hairpin 2, while in the minor pathway the intermediate consisted of hairpin 2 and the helix. Each run proceeded through one and only one intermediate, and the major pathway was observed in twice as many runs. It appears that the pathways observed in our simulation are consistent with available experimental data on Protein G - this will be discussed at length elsewhere, and does not bear significantly on the present work.

The existence of a folding intermediate in our simulation of Protein G, while complicating our analysis somewhat, has one important advantage: we are able to see that the kinetics of only half of the sidechains are sensitive to the presence of the intermediate; the other residues exhibit single-exponential relaxation. In other words, a kinetic intermediate can be completely invisible if the wrong position is used to probe folding. We observed a distribution of residue relaxation rates for both the pre- and post-intermediate steps. Each of these steps is a purely two-state process as seen by the abrupt jump in rms deviation and energy. It appears, then, that a few key residues reach nativity faster than all others and propel the chain through its transition state. Further relaxation after the major event via backbone fluctuations yields a distribution of rates over the fold, the exact nature of which is governed by the extent of backbone mobility at each position in the ensemble.

At first glance this observation runs contrary to the belief that in two-state transitions all parts of the structure must reach nativity at the same rate. The argument goes that if structure is obtained gradually, with some parts folding faster than others, then there are many distinct ensembles of states for the chain to traverse. To dispell this fear, it is crucial to note that the core residues which

are observed in simulation to freeze fastest also happen to be in key organizing positions. The ensemble of conformations consistent with their freezing is highly native and therefore extremely small compared with the ensemble of unfolded conformations. The major transition of protein folding occurs between these two ensembles and is a two-state transition in simulation as in reality. The entire molecule does not, however, necessarily reach equilibrium concomitantly with this barrier crossing. There can be many other smaller barriers associated with backbone fluctuations which need to be crossed in order for all sidechains to reach equilibrium (see Figure 13).

It is important to note that temperature plays a key role in making sidechain relaxation possible in a reasonable amount of time. At low temperatures backbone fluctuations are small and sidechain relaxation is a very noticeable and very long process, as seen in Figure 7. At optimal folding temperature, however, the energy of the post-nucleation ensemble is very close to its equilibrium value. Sidechain relaxation is still very slow, following stretched-exponential kinetics, but the product of the major transition is significantly closer energetically (and therefore structurally) to equilibrium. This suggests that under optimal conditions, the slow sidechain packing process may not be physiologically relevant because the ensemble of folded yet unequilibrated molecules is structurally close enough to the native ensemble that it may exhibit similar amounts of protection from proteolysis. The relatively small gap between mispacked and native molecules at these temperatures suggests that relevant experiments must be sensitive enough to detect such differences.

Since we could not observe full equilibration in the all-atom simulation, we return to the lattice simulations in order to discuss the relevant post-nucleation processes which establish equilibrium. In lattice simulations we found that the dynamics during short times is reminiscent of the classic nucleation mechanism that has been observed before.<sup>18</sup> Due to the existence of sidechain states, the nucleation-organized backbone does not reach equilibrium immediately. At long times the

system can end up in traps which require some degree of backbone motion to allow sidechains to interconvert. This suggests that perhaps the energy landscape after the native fold has been acquired consists of a series of barriers, associated with backbone fluctuations, which must be crossed. As the system traverses these barriers it moves to lower and lower energies. If one assumes that the transition states for these barriers are largely very similar, the resulting relaxation process can be shown to be logarithmic in time.<sup>37</sup> In the lattice simulations, we observed a highly stretched exponential relaxation at long times. Since the stretching exponent is very low at 0.09, the time dependence of energy is essentially logarithmic. The landscape for slow sidechain equilibration thus seems to be one of increasingly deeper wells, rather than a single cooperative transition to nativity. This places sidechain relaxation within the set of phenomena that can be characterized as a glass. Classic lattice models without sidechain states, however, do not exhibit a glass transition at any reasonable temperature.<sup>8</sup> Our lattice simulations indicate that the presence of sidechain degrees of freedom may lead to glassy relaxation, but further detailed characterization of the energy landscape, as well as additional tests using more realistic models, are required to solidify this claim.

Using both all-atom and lattice simulations, we have demonstrated that full sidechain relaxation during protein folding can be a process whose timescale is significantly slower than that of crossing the major folding barrier. While the major barrier is traversed via the classic nucleation mechanism, we find that equilibrium is reached via a set of smaller barrier crossings that correspond to backbone fluctuations. The heterogeneities inherent in protein structures give rise to a distribution of sidechain relaxation times which can span up to an order of magnitude. A number of recent experiments are consistent with our findings. We hope that this work will spur further dialogue between simulations and experiments to elucidate the complex processes that bring sidechains to equilibrium.

## Methods

**Lattice Model with Internal Monomer States.** We use a standard three-dimensional lattice model in which each monomer occupies a single lattice site. For the 27-mer simulations, a sequence was designed to fold to a unique native conformation as described in.<sup>38</sup> For the 48-mer simulation, a fast-folding sequence was obtained from a lattice protein evolution study described in.<sup>20</sup> The standard Miyazawa-Jernigan parameter set<sup>39</sup> is used to compute the energy of a conformation. Two monomers are said to be in contact if they are nearest neighbors on the lattice, and are not sequence neighbors. Additionally, each monomer has  $n$  internal states, where  $n$  is a parameter of the model. We present data for 27-mer folding with  $n = 1, 2, 4,$  and  $8,$  and for 48-mer folding with  $n = 1, 2,$  and  $4.$  The internal state of each monomer is stored as a number from  $0$  to  $n - 1.$  The  $0$  state is the native state, while the states  $1..n - 1$  are non-native. If  $n = 1$  then all monomers remain native throughout the simulation, and the model is equivalent to the standard lattice model. Non-native monomers do not contribute to energy. That is, two monomers in contact will contribute to energy only if they are both in their native state, the  $0$  state.

The standard cubic lattice move-set<sup>40</sup> is used to evolve the backbone conformation, and a Metropolis criterion<sup>41</sup> with temperature  $T$  is used to accept/reject moves. In addition to backbone moves, the internal states of the monomers must be evolved. After each backbone move is attempted, we attempt  $n - 1$  internal state moves. At each such move, a random monomer is chosen. If the monomer is making more than  $c$  contacts with other monomers, its internal state is not allowed to change. Otherwise, its internal state is randomly flipped to one of the other  $n - 1$  states, the change in energy of the conformation is computed, and the move is accepted/rejected based on the Metropolis criterion. The parameter  $c$  can take the values  $0$  through  $4.$  When  $c = 4,$

internal states can interchange freely and are not affected by the conformation of the backbone. If  $c = 0$ , internal states can interchange only if the monomer makes no contacts. In this study we take  $c = 0$  throughout, except in the control simulation (Figure 2D) in which we use  $c = 4$ . Folding simulations are started from random backbone conformations generated by an infinite temperature simulation. The internal state of each monomer is initialized randomly.

**All-Atom Protein Folding Simulations.** The all-atom Monte Carlo simulation previously described in<sup>24</sup> was used to fold protein G (pdb code: 1IGD). By representing all sidechain and backbone heavy atoms as hard spheres, the protein was simulated as a polymer with excluded volume interactions, where chain crossings are strictly prohibited. The energy of a conformation was computed as  $E = E_G + E_h$ , where (1) the atom-atom G $\bar{o}$  energy  $E_G = \sum C(A, B)\Delta(A, B)$ , with  $\Delta(A, B) = 1$  if the heavy atoms  $A$  and  $B$  were in contact and zero otherwise,  $C(A, B)$  was -1 if  $A$  and  $B$  were in contact in the native conformation, 1 if they were not, and  $\infty$  if they were sterically clashed and (2) the backbone hydrogen bonding energy  $E_h = N_h h$ , where  $N_h$  corresponds to the number of amide N-carbonyl O pairs in contact.  $h$  was chosen to be -0.6 in order to match experimental stabilities of the protein G helix and hairpins taken in isolation (JS and EIS, manuscript in preparation).

The torsional move set ensures that canonical bond lengths and geometries (including planar peptide bonds) are maintained throughout the entire simulation. Backbone and sidechain moves consisted of concerted random rotations of backbone  $\phi/\psi$  and sidechain  $\chi$  angles, respectively. 10 sidechain moves were completed for each backbone move in order to allow sufficient relaxation of sidechain geometries after a change in the backbone topology.

50 folding simulations were initiated from random coil conformations, obtained by simulating the native state with only the excluded volume interaction turned on. The temperature was then

quenched to  $T=1.575$  and the chain was allowed to equilibrate for  $2 \times 10^9$  MC steps, where 1 MC step consisted of 1 backbone and 10 sidechain moves. Given the experimentally measured transition temperature of  $360K$  and our simulation transition temperature of 1.95,  $T=1.575$  corresponds to an actual temperature of  $\approx 290$  K.

From the 50 trajectories of protein G, we estimated the probability to fold<sup>42</sup> ( $p_{\text{fold}}$ ) of conformations observed just prior to reaching the native state, by counting the number of times the native state was attained from the selected conformation in 20 separate runs of  $10 \times 10^6$  MC steps.

**Fitting of residue relaxation curves.** After collecting many long runs, we averaged the internal sidechain state of each monomer at each time step over all runs, assigning 1 if the residue was native, and 0 otherwise. For lattice simulations, 130 runs were used, and a two-state exponential fit of the form  $f(x) = a_0 + a_1 \exp(-a_2 t)$  was very good for all residues. For all-atom simulations, 50 runs were used, and averaging over runs was performed by assigning 1 to each residue whose  $\chi$ -angles were all within  $60^\circ$  of the native angles, and 0 otherwise. A value of 1 thus corresponded to observing the native rotamer. Fits to a three-state model were performed as described in Results. All fits were done using the nonlinear least-squares Marquardt-Levenberg algorithm.

## Acknowledgements

We would like to thank Leonid Mirny and Phillip Geissler. Research was supported by NIH grant GM52126.



## References

1. Brooks, C. L., Karplus, M. & Pettitt, B. M. (1988). *Proteins: A Theoretical Perspective of Dynamics, Structure, and Thermodynamics*. John Wiley & Sons, New York.
2. Richards, F. M. & Lim, W. A. (1994). An analysis of packing in the protein folding problem. *Quat. Rev. Biophys.* **26**, 423–498.
3. Heringa, J. & Argos, P. (1999). Strain in protein structures as viewed through nonrotameric side chains: I. their position and interaction. *Proteins* **37**, 30–43.
4. Levitt, M., Gerstein, M., Huang, E., Subbiah, S. & Tsai, J. (1997). Protein folding: The endgame. *Annu. Rev. Biochem.* **66**, 549–579.
5. Dunbrack, R. L. & Karplus, M. (1994). Conformational-analysis of the backbone-dependent rotamer preferences of protein side-chains. *Nature Struct. Biol.* **1**, 334–340.
6. Fersht, A. (1999). *Structure and Mechanism in Protein Science*. W. H. Freeman and Company, New York, 1st ed.
7. Shakhnovich, E. I. & Finkelstein, A. V. (1989). Theory of cooperative transitions in protein molecules. i. why denaturation of globular proteins is a first-order phase transition. *Biopolymers* **28**, 1667–1680.
8. Gutin, A., Sali, A., Abkevich, V., Karplus, M. & Shakhnovich, E. I. (1998). Temperature dependence of the folding rate in a simple protein model: Search for a "glass" transition. *J. Chem. Phys.* **108**, 6466–6483.

9. Bryngelson, J. D. & Wolynes, P. G. (1989). Intermediates and barrier crossing in a random energy-model (with applications to protein folding). *J. Phys. Chem.* **93**, 6902–6915.
10. Steinbach, P. J. & Brooks, B. R. (1994). Protein simulation below the glass-transition temperature - dependence on cooling protocol. *Chem. Phys. Lett.* **226**, 447–452.
11. Vitkup, D., Ringe, D., Petsko, G. A. & Karplus, M. (2000). Solvent mobility and the protein 'glass' transition. *Nature Struct. Biol.* **7**, 34–38.
12. Lee, A. L. & Wand, J. (2001). Microscopic origins of entropy, heat capacity and the glass transition in proteins. *Nature* **411**, 501–504.
13. Gō, N. & Abe, H. (1981). Noninteracting local-structure model of folding and unfolding transition in globular proteins. i. formulation. *Biopolymers* **20**, 991–1011.
14. Bromberg, S. & Dill, K. A. (1994). Side-chain entropy and packing in proteins. *Protein Sci.* **3**, 997–1009.
15. Klimov, D. K. & Thirumalai, D. (1998). Cooperativity in protein folding, from lattice models with sidechains to real proteins. *Folding & Design* **3**, 127–139.
16. Li, L., Mirny, L. A. & Shakhnovich, E. I. (2000). Kinetics, thermodynamics, and evolution of non-native interactions in protein folding nucleus. *Nature Struct. Biol.* **7**, 336–342.
17. Kussell, E., Shimada, J. & Shakhnovich, E. I. (2001). Excluded volume in protein side-chain packing. *J. Mol. Biol.* **311**, 183–193.
18. Abkevich, V. I., Gutin, A. M. & Shakhnovich, E. I. (1994). Specific nucleus as the transition state for protein folding: Evidence from the lattice model. *Biochemistry* **33**, 10026–10036.

19. Shakhnovich, E., Abkevich, V. & Ptitsyn, O. (1996). Conserved residues and the mechanism of protein folding. *Nature* **379**, 96–98.
20. Mirny, L. A., Abkevich, V. & Shakhnovich, E. I. (1998). How evolution makes proteins fold quickly. *Proc. Natl. Acad. Sci. USA* **95**, 4976–4981.
21. McCallister, E. L., Alm, E. & Baker, D. (2000). Critical role of beta-hairpin formation in protein g folding. *Nature Struct. Biol.* **7**, 669–673.
22. Nauli, S., Kuhlman, B. & Baker, D. (2001). Computer-based redesign of a protein folding pathway. *Nature Struct. Biol.* **8**, 602–605.
23. Park, S., Shastry, M. C. R. & Roder, H. (1999). Folding dynamics of the b1 domain of protein g explored by ultrarapid mixing. *Nature Struct. Biol.* **6**, 943–947.
24. Shimada, J., Kussell, E. & Shakhnovich, E. I. (2001). The folding thermodynamics and kinetics of crambin using an all-atom monte carlo simulation. *J. Mol. Biol.* **308**, 79–95.
25. Bolhuis, P. G., Chandler, D., Dellago, C. & Geissler, P. L. (2002, submitted). Transition path sampling: Throwing ropes over rough mountain passes, in the dark. *Annu. Rev. Phys. Chem.* .
26. Fersht, A. R. (1995). Optimization of rates of protein-folding - the nucleation-condensation mechanism and its implications. *Proc. Natl. Acad. Sci. USA* **92**, 10869–10873.
27. Sosnick, T. R., Mayne, L. & Englander, S. W. (1996). Molecular collapse: The rate-limiting step in two-state cytochrome c folding. *Proteins* **24**, 413–426.

28. Shakhnovich, E. I. (1997). Theoretical studies of protein-folding thermodynamics and kinetics. *Curr. Opin. Struct. Biol.* **7**, 29–40.
29. Pande, V. S., Grosberg, A. Y., Tanaka, T. & Rokhsar, D. S. (1998). Pathways for protein folding: is a new view needed? *Curr. Opin. Struct. Biol.* **8**, 68–79.
30. Englander, S. W. (2000). Protein folding intermediates and pathways studied by hydrogen exchange. *Annu. Rev. Biophys. Biomol. Struct.* **29**, 213–238.
31. Staniforth, R. A., Dean, J. L. E., Zhong, Q., Zerovnik, E., Clarke, A. R. & Waltho, J. P. (2000). The major transition state in folding need not involve the immobilization of side chains. *Proc. Natl. Acad. Sci. USA* **97**, 5790–5795.
32. Ha, J. & Loh, S. N. (1998). Changes in side chain packing during apomyoglobin folding characterized by pulsed thiol-disulfide exchange. *Nature Struct. Biol.* **5**, 730–737.
33. Sridevi, K., Juneja, J., Bhuyan, A. K., Krishnamoorthy, G. & Udgaonkar, J. B. (2000). The slow folding reaction of barstar: the core tryptophan region attains tight packing before substantial secondary and tertiary structure formation and final compaction of the polypeptide chain. *J. Mol. Biol.* **302**, 479–495.
34. Alexandrov, V. Y. (1977). *Cells, Molecules, and Temperature: Conformational Flexibility of Macromolecules and Ecological Adaptation..* Springer-Verlag, New York.
35. Zavodszky, P., Kardos, J., Svingor, A. & Petsko, G. A. (1998). Adjustment of conformational flexibility is a key event in the thermal adaptation of proteins. *Proc. Natl. Acad. Sci. USA* **95**, 7406–7411.

36. Abkevich, V. I., Gutin, A. M. & Shakhnovich, E. I. (1994). Free energy landscape for protein folding kinetics: Intermediates, traps, and multiple pathways in theory and lattice model simulations. *J. Chem. Phys.* **101**, 6052–6062.
37. Shakhnovich, E. I. & Gutin, A. M. (1989). Relaxation to equilibrium in the random energy model. *Europhys. Lett.* **9**, 569–574.
38. Morrissey, M. & Shakhnovich, E. I. (1996). Design of proteins with selected thermal properties. *Folding & Design* **1**, 391–406.
39. Miyazawa, S. & Jernigan, R. (1985). Estimation of effective interresidue contact energies from protein crystal structures: quasi-chemical approximation. *Macromolecules* **18**, 534–552.
40. Sali, A., Shakhnovich, E. I. & Karplus, M. (1994). Kinetics of protein folding. a lattice model study for the requirements for folding to the native state. *J. Mol. Biol.* **235**, 1614–1636.
41. Metropolis, N., Rosenbluth, A. W., Rosenbluth, M. N., Teller, A. H. & Teller, E. (1953). Equation of state calculations by fast computing machines. *J. Chem. Phys.* **21**, 1087–1092.
42. Du, R., Pande, V. S., Grosberg, A. Y., Tanaka, T. & Shakhnovich, E. I. (1998). On the transition coordinate for protein folding. *J. Chem. Phys.* **108**, 334–350.

# Figures

## Figure 1

Thermodynamics of 27-mer and 48-mer lattice models. Each point corresponds to an average of energy over a lattice simulation started at the native state. Each simulation was run for  $3 \times 10^8$  steps and energy was sampled every  $3 \times 10^5$  steps. The correlation time of energy was found to be much less than our sampling interval at all temperatures. The number of internal sidechain states for each model is indicated by the color and shape of the points, as in the legend. Fits to a two-state thermodynamic model are given in solid lines colored to match the corresponding lattice model that was used. Parameters for these fits are given in Table 1.

## Figure 2

Kinetics of 27-mer lattice models. In panels **A**, **B**, and **C**, the kinetics of the models with 2, 4, and 8 sidechain states per monomer are shown. Interconversion of internal sidechain states in these models can take place only if a given monomer is not in contact with any other monomer. The logarithm of the mean first passage time (MFPT) to native energy is shown by open circles, while the average time for reaching a stable native backbone is given by squares. By stable formation of the backbone we mean that once formed, the backbone did not subsequently unfold by more than 50% before reaching the native energy. In panel **D**, two control models are shown: the  $n = 1$  model, in which each monomer has a single internal state, and thus corresponds to the classic lattice model; and the  $n = 2$  unhindered model, in which monomers have 2 sidechain states, and these states can interconvert freely, regardless of whether the given monomer is in contact with others or not. Each point was calculated over a set of between 100 and 200 runs, and error bars corresponding to 1.5 standard deviations are indicated.

### Figure 3

Kinetics of the 48-mer model with 4 internal states per monomer. Panel **A** indicates the MFPT for reaching native energy by circles, and the average time to reach the stable native backbone by squares. Panel **B** shows the time to reach the stable backbone with diamonds, and the amount of time to go from the native backbone to the native energy with x-marks.

### Figure 4

Average time traces for two representative residues in the lattice 48-mer. Residue 35 is a nucleus residue exhibiting fast freezing, while residue 13 is a non-nucleus residue with an average freezing rate. The black line is the best single-exponential fit to the data.

### Figure 5

Histogram of residue relaxation rates for 48-mer with 4 internal states. Histograms for low temperature ( $T = 7.4$ ) and optimal folding temperature ( $T = 9.1$ ) are shown. Each residue was assigned a value of 1 if it was in its native sidechain state, and 0 otherwise, and these numbers were averaged at each time step over 130 long runs. Rates were calculated by fitting a single exponential relaxation to the resulting native occupancy curves for each residue. At  $T = 7.4$ , runs of length  $2 \times 10^9$  were used; at  $T = 9.1$ , run length was  $2 \times 10^8$ . The fast positions at each temperature are labelled by numbers on the histograms. Red numbers correspond to positions which are more than 90% ordered in the native state, while green numbers are less than 90% ordered.

### Figure 6

Lattice 48-mer structure colored by rate of freezing at  $T = 7.4$ . Nucleus positions, determined in,<sup>19</sup>

are indicated by large spheres. Colors range from white (slow-freezing) to blue (fast-freezing).

### Figure 7

Relaxation of energy to equilibrium. By averaging energy at each time step over 130 long runs, we obtained energy relaxation curves at temperatures 7.4 and 9.1. The same runs were used in Figure 5. The green curves in each figure are the average energy obtained from simulations. The red line corresponds to the average energy at equilibrium, and was obtained for each temperature by averaging over a long run started at the native lowest energy state, as in Figure 1. The dashed line is a fit to a three-state exponential model (see Methods). A fit using a two-state exponential model yielded a nearly identical curve. The arrows indicate the average time to reach the stable native backbone at each temperature. The solid curve in panel **B** is a two-phase fit using a single exponential ( $a_0 + a_1 \exp(-a_2 t / 10^8)$ ) for short times, and a stretched exponential ( $-1092 + b_1 \exp(-b_2 t^\alpha)$ ) for long times. Parameters of these fits are  $a_0 = -838$ ,  $a_1 = 663$ ,  $a_2 = 235$ ,  $b_1 = 9.5 \times 10^5$ ,  $b_2 = 12.1$ , and  $\alpha = 0.087$ . The value of  $-1092$  for the equilibrium energy corresponds to the red line.

### Figure 8

Average time traces for two representative residues in Protein G. P30 and P52 are typical two-state and three-state residues, respectively. The black line is the best fit as described in Tables 2 and 3.

### Figure 9

Protein G residues exhibiting fastest two-state relaxation to a highly ordered state. The four fastest residues whose relaxation curves fit well to a two-state kinetic model, and whose equilibrium conformation is at least 70% ordered are shown in pink. These residues occupy key positions in the



major-pathway intermediate that is seen in all-atom simulations of Protein G folding. The helical residue F30 is lodged between L5 of beta-strand 1, and T18 of beta-strand 2, thus organizing the entire structure of the intermediate which consists of hairpin 1 and the helix. T25 makes contacts at the hairpin-helix turn.

#### Figure 10

Protein G residues exhibiting fastest three-state relaxation to highly ordered state. Residues V6, F52, and V54, shown in pink, exhibited fastest three-state relaxation, and remained highly ordered at equilibrium. All three are important post-intermediate positions: F52 and V54 secure strand 4 of hairpin 2 to the helix, while V6 makes contacts between the two hairpins.

#### Figure 11

Dependence of residue nativity upon  $p_{\text{fold}}$ . Conformations were binned according to their  $p_{\text{fold}}$  values, and the average change in number of contacts, with respect to the  $p_{\text{fold}} = 0$  state, is plotted for each residue. Each curve corresponds to an average over all conformations within the given range of  $p_{\text{fold}}$  values.

#### Figure 12

Dependence of specific contacts upon  $p_{\text{fold}}$ . As in Figure 11, conformations were binned according to their  $p_{\text{fold}}$  values. For each  $p_{\text{fold}}$  range, the average change (with respect to the  $p_{\text{fold}} = 0$  state) in number of atom-atom contacts between all pairs of residues that make native contacts, is plotted for each pair of residues. Residues pairs are arbitrarily ordered in a linear fashion along the x-axis.

### Figure 13

Schematic diagram of barriers and their significance during the folding reaction. The first barrier corresponds to the nucleation event which organizes the backbone topology. Associated with this barrier is the freezing of a small group of residues - the nucleus - into their native sidechain states (blue dots). Other residues may still be partially disordered (red dots). The disordered residues become increasingly native-like via barriers corresponding to backbone fluctuations which momentarily free a few residues (see small arrows), and allow their sidechain states to interchange. Barriers become higher as chain approaches equilibrium.

n	$a_0$	$a_1$	$a_2$
27-mer			
1	-111	518	16.9
2	-71.7	500	23.4
4	-44.2	433	26.3
8	-18.2	320	24.0
48-mer			
1	-82	263	13.8
2	-3.6	222	16.0
4	38	151	14.2

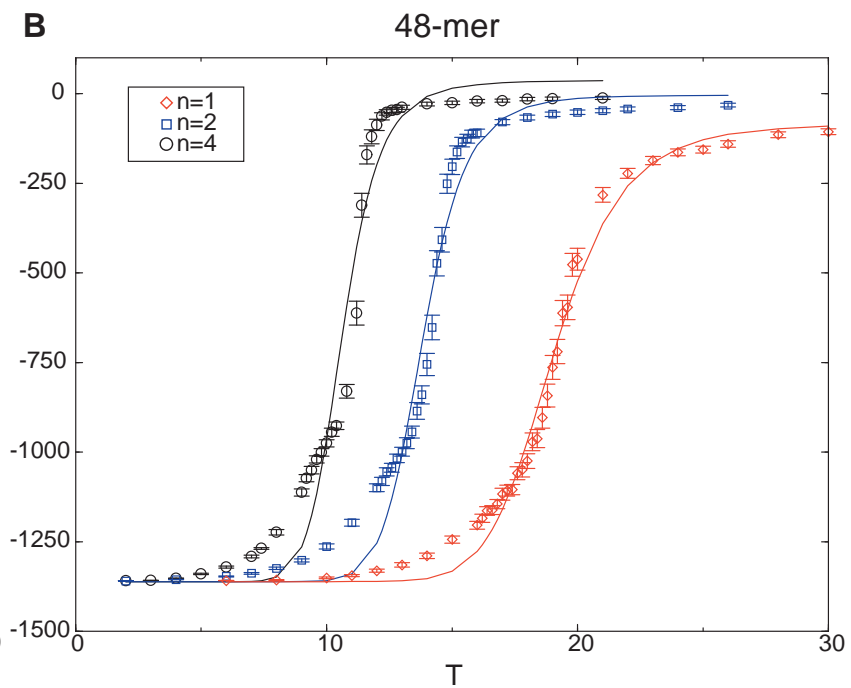
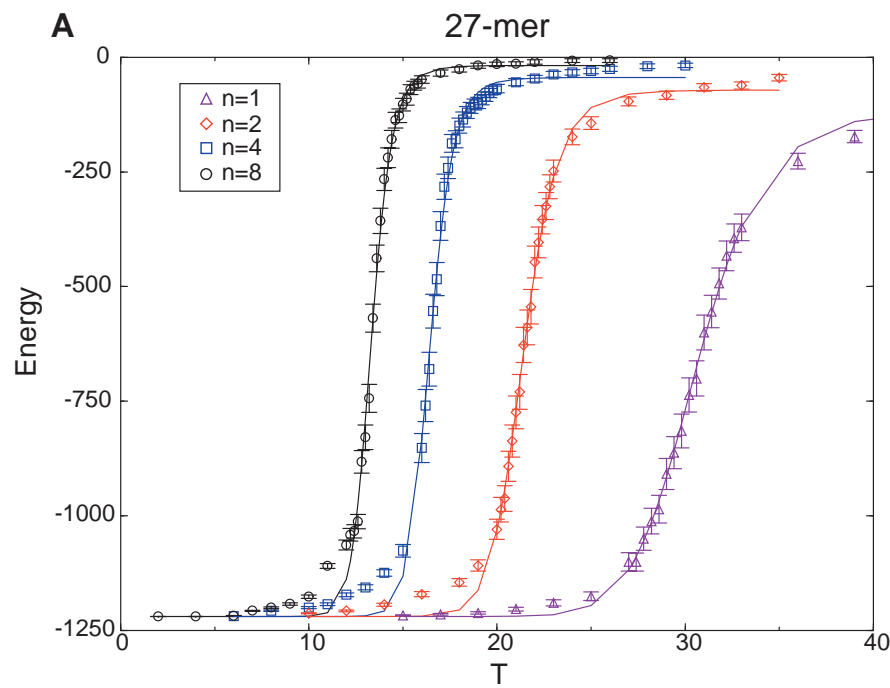
Table 1: Two-state Fits to Thermodynamic Data. Thermodynamics shown in Figure 1 was fit using the form  $f(x) = a_3 + (a_0 - a_3) \exp(a_2 - a_1/T)/(1 + \exp(a_2 - a_1/T))$ , where  $a_3$  is the native state energy for each model. For the 27-mer,  $a_3 = -1219$ ; for the 48-mer,  $a_3 = -1361$ .

#	$a$	$b$	$c$	$d$	err $a$	err $b$
13K	0.174	-	0.064	0.094	$\pm$ 0.009	-
49T	0.190	-	0.150	0.483	0.008	-
<b>37N</b>	0.756	-	0.603	0.826	0.003	-
36D	0.779	-	0.168	0.326	0.01	-
15E	0.791	-	0.302	0.368	0.005	-
<b>7I</b>	0.941	-	0.676	0.965	0.003	-
<b>21V</b>	1.027	-	0.357	0.739	0.007	-
<b>0V</b>	1.035	-	0.379	0.813	0.01	-
24E	1.159	-	0.011	0.060	0.2	-
32Q	1.159	-	0.110	0.198	0.02	-
27E	1.283	-	0.442	0.539	0.008	-
<b>33Y</b>	1.308	-	0.810	0.991	0.003	-
31K	1.365	-	0.444	0.501	0.007	-
<b>16T</b>	1.504	-	0.606	0.958	0.005	-
<b>3Y</b>	1.581	-	0.779	1.000	0.003	-
<b>17T</b>	1.626	-	0.544	0.884	0.006	-
<b>5L</b>	1.724	-	0.636	1.000	0.004	-
22D	1.809	-	0.423	0.554	0.01	-
28K	1.882	-	0.026	0.057	0.00	-
<b>18T</b>	1.891	-	0.632	0.991	0.005	-
<b>25T</b>	1.931	-	0.596	0.985	0.005	-
<b>30F</b>	2.068	-	0.723	1.000	0.004	-

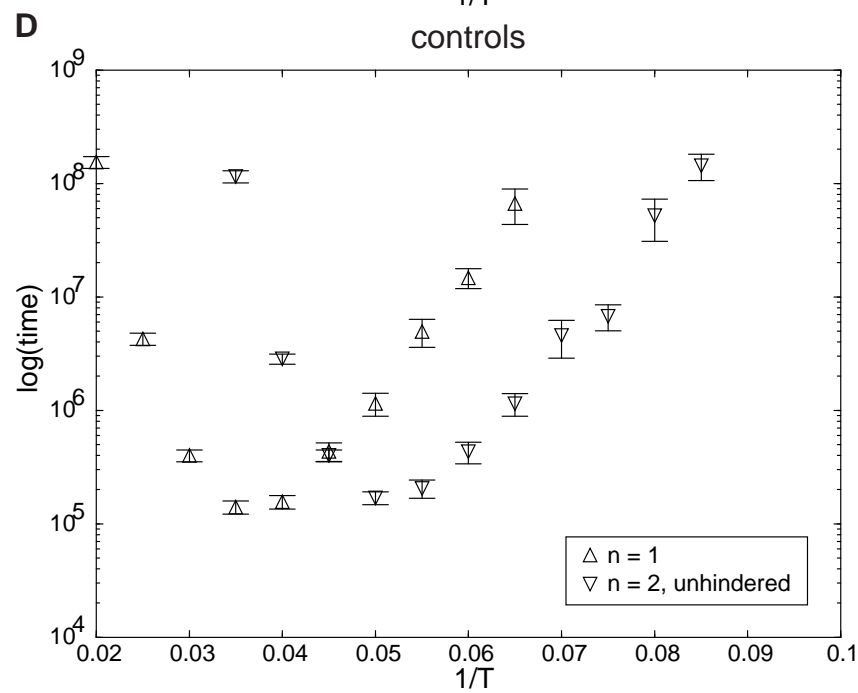
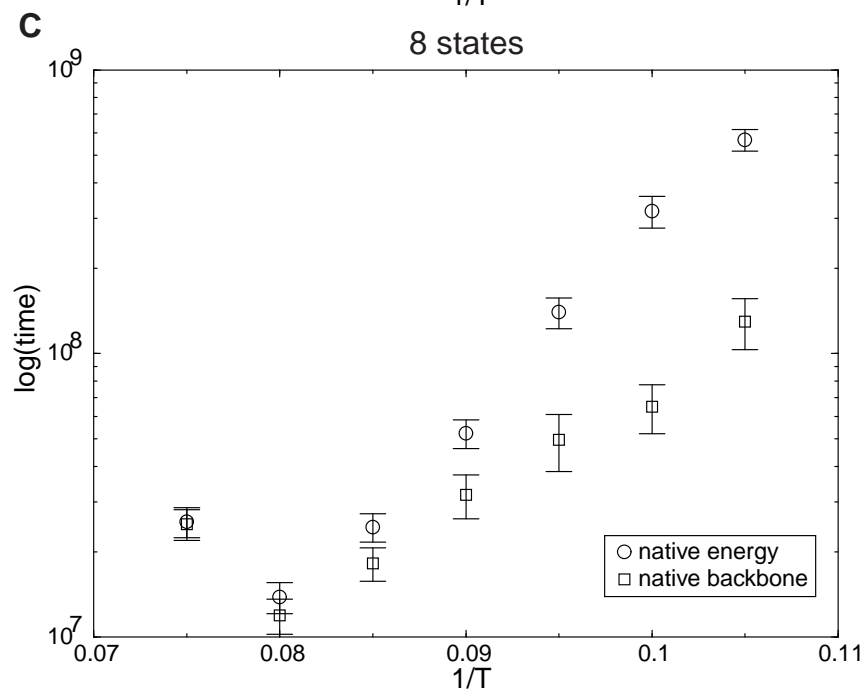
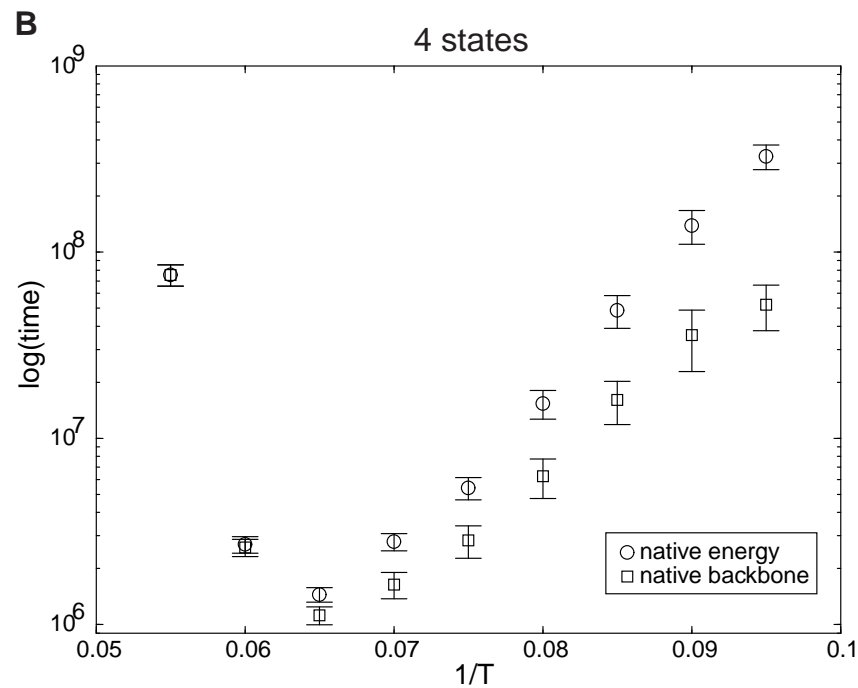
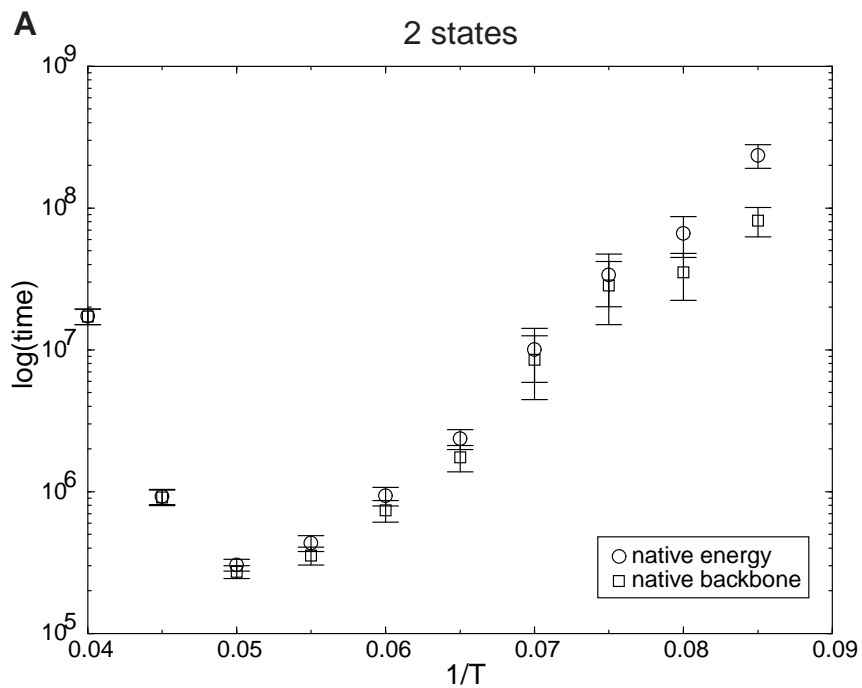
Table 2: Two-State Residues and Fits for Protein G. Individual residue relaxation curves were initially fit to the following three-state kinetic model:  $f(x) = d + c(a/(b - a))exp(-bx/10^9) - c(b/(b - a))exp(-ax/10^9)$ . The parameter  $d$ , corresponding to fully equilibrated value of residue ordering, was obtained from long equilibrium simulation, and was not varied in the fitting process. Standard non-linear fitting was used to calculate  $a$ ,  $b$ , and  $c$ . The residues listed in this table had one rate constant that was at least an order of magnitude faster than the other. The fits listed are therefore essentially two-state fits, and we report only the relevant slow rate constant. The three-state model was used in order to determine which residues were markedly two-state, and which ones were not. Asymptotic error on parameter  $a$  is listed as well. The table is sorted by the rate constant  $a$ .

#	$a$	$b$	$c$	$d$	err $a$	err $b$
<b>12L</b>	0.279	1.974	0.601	0.842	$\pm 0.008$	$\pm 0.1$
8N	0.328	2.538	0.136	0.254	0.02	0.6
46D	0.464	2.524	0.058	0.191	0.07	1.0
<b>55T</b>	0.710	2.158	0.384	0.710	0.02	0.2
35N	0.722	3.301	0.034	0.187	0.1	1.8
47D	0.834	1.387	0.130	0.294	0.2	0.5
<b>1T</b>	0.859	5.414	0.426	0.780	0.01	0.3
4K	1.018	9.252	0.178	0.210	0.01	1.1
10K	1.02	1.02	0.027	0.053	0.03	0.03
42V	1.127	1.127	0.180	0.508	0.01	0.01
50K	1.205	1.205	0.369	0.386	0.004	0.004
56E	1.319	1.319	0.610	0.666	0.003	0.003
44T	1.361	1.361	0.341	0.689	0.006	0.006
<b>43W</b>	1.623	3.455	0.750	1.000	0.01	0.06
<b>39V</b>	1.719	1.719	0.567	0.984	0.004	0.004
<b>45Y</b>	1.734	1.734	0.883	0.999	0.002	0.002
<b>53T</b>	1.749	1.749	0.517	0.850	0.005	0.005
<b>51T</b>	2.020	2.020	0.510	0.841	0.006	0.006
<b>54V</b>	2.034	2.034	0.687	1.000	0.003	0.003
<b>6V</b>	2.035	2.035	0.642	0.966	0.004	0.004
<b>52F</b>	2.039	2.039	0.858	1.000	0.002	0.002
19K	2.111	3.089	0.049	0.068	0.4	0.9
40D	2.198	2.198	0.037	0.170	0.07	0.07
2T	2.923	2.923	0.285	0.628	0.02	0.02

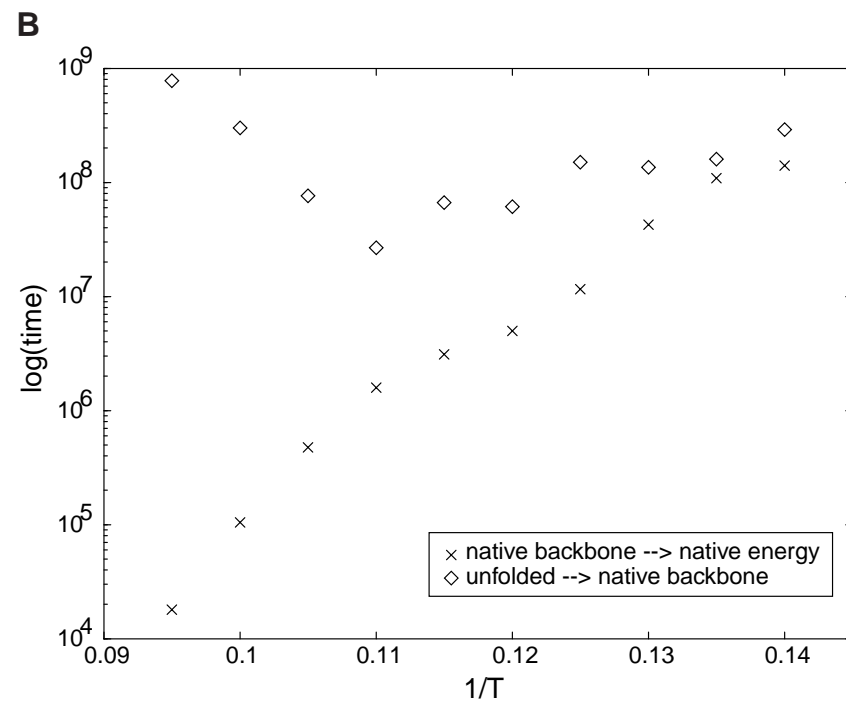
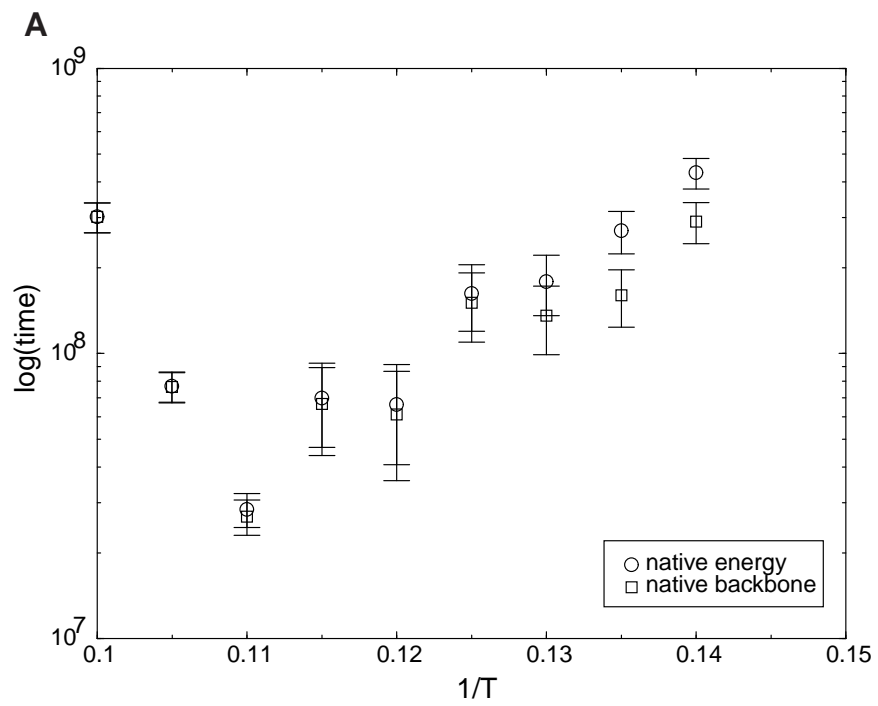
Table 3: Three-State Residues and Fits for Protein G. Fits were performed as in Table 2. The two rate constant obtained for the residues listed here were within one order of magnitude of each other. The table is sorted by the slower of the two rate constants, which is arbitrarily designated to be parameter  $a$ .





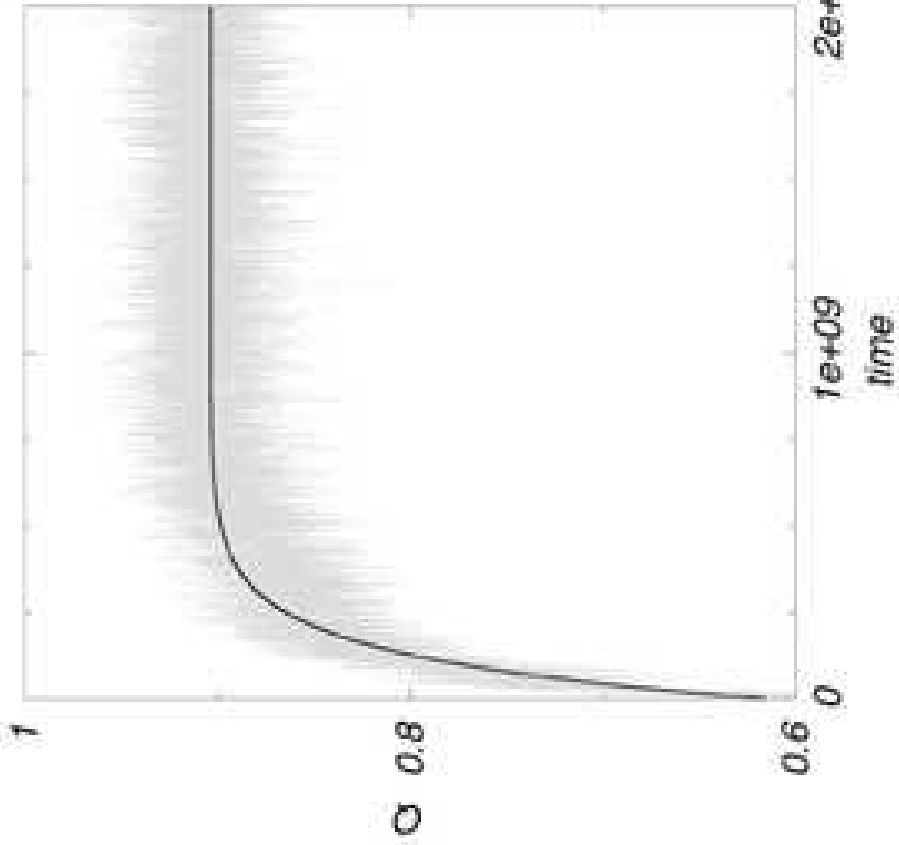




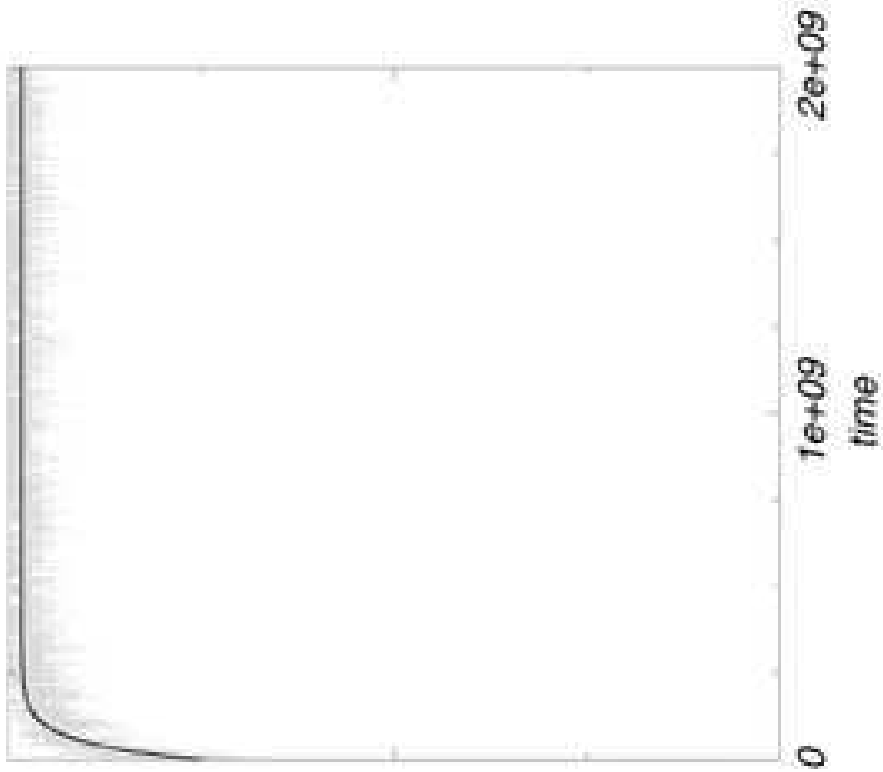


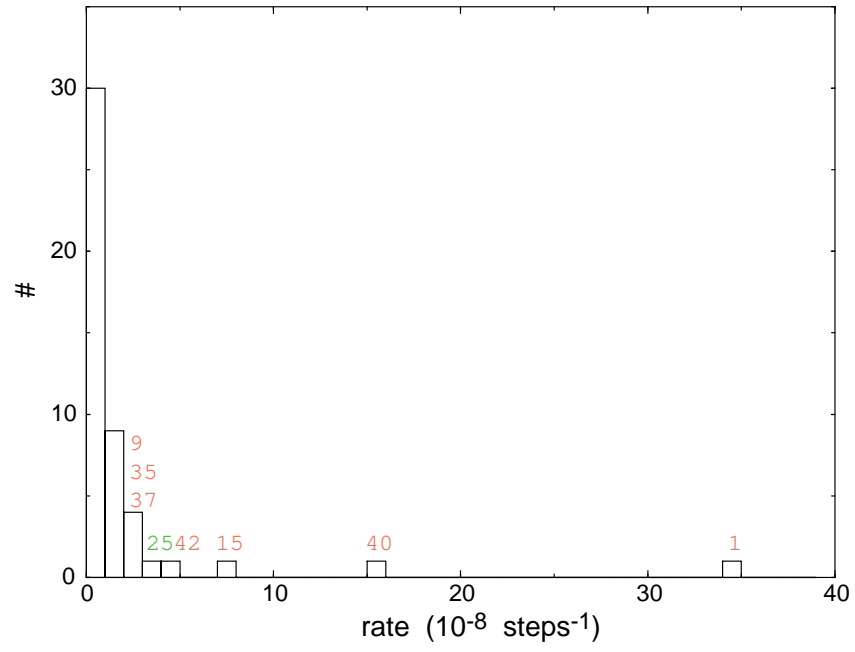
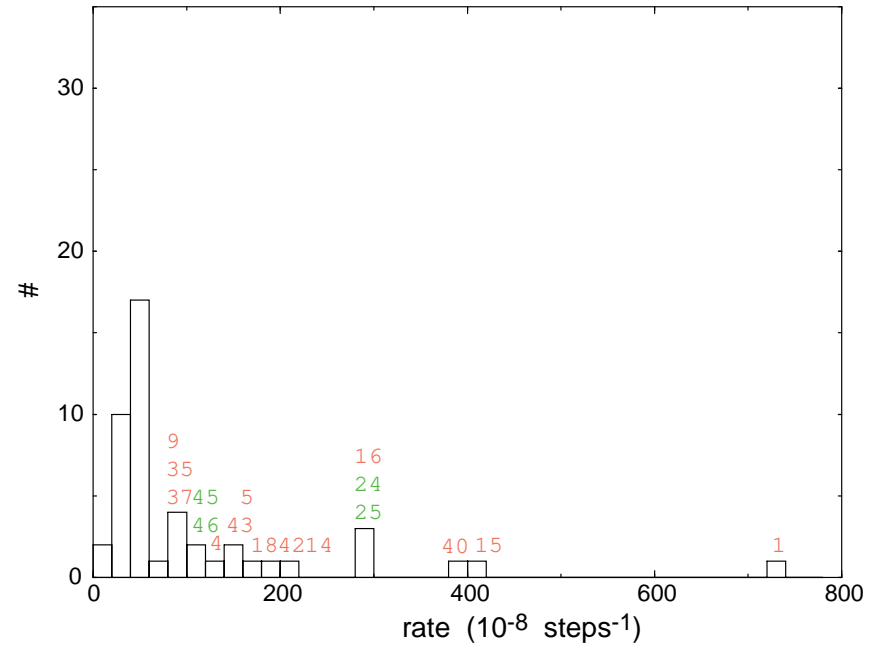
48-mer, 4 states

Residue 13



Residue 35



**A****T = 7.4****B****T = 9.1**

**Legend**



Fast Freezing

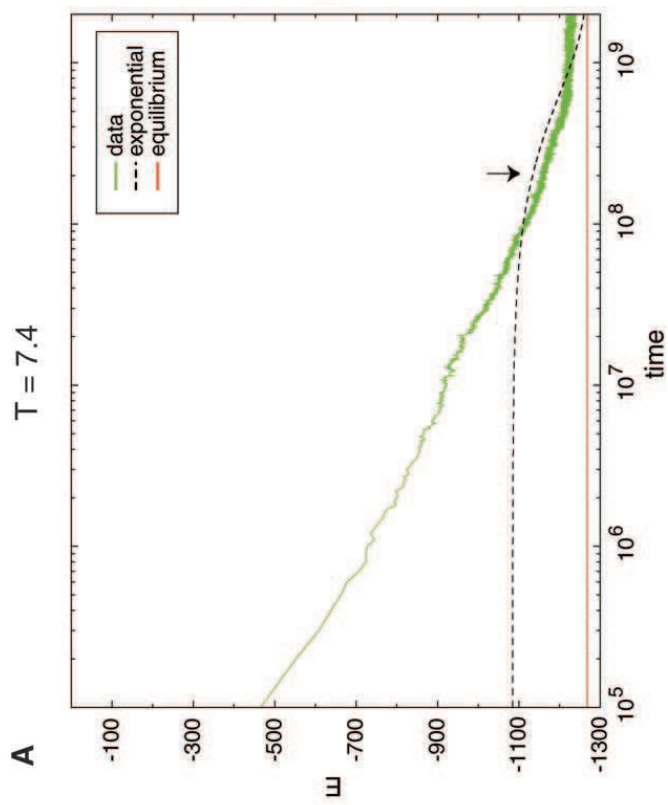
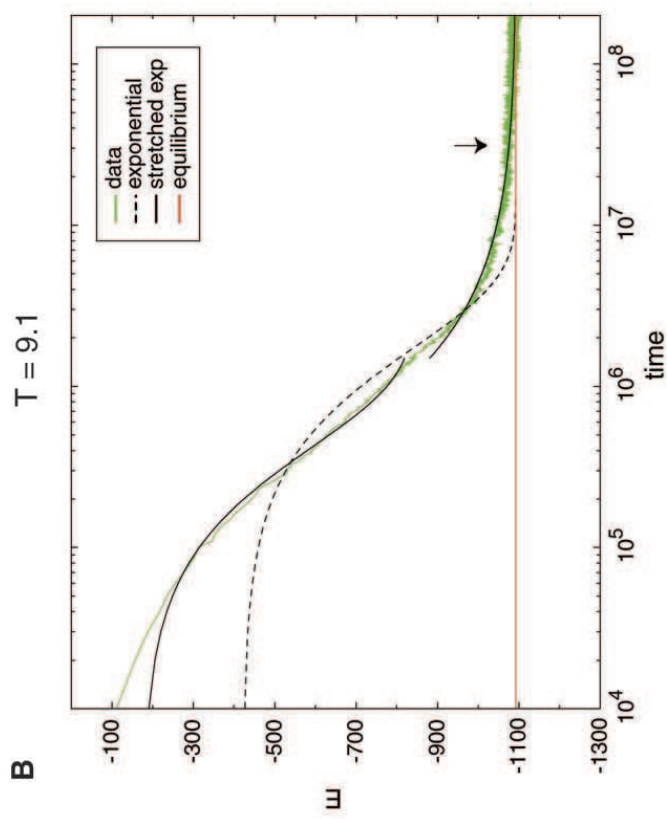


Slow Freezing

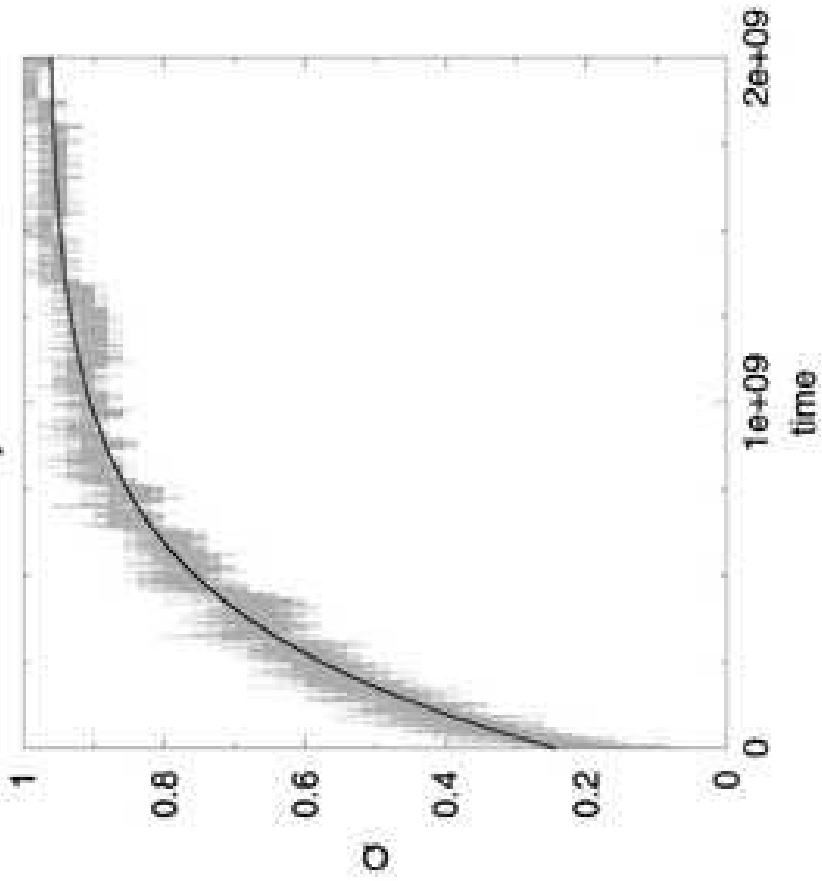


Nucleus Residue

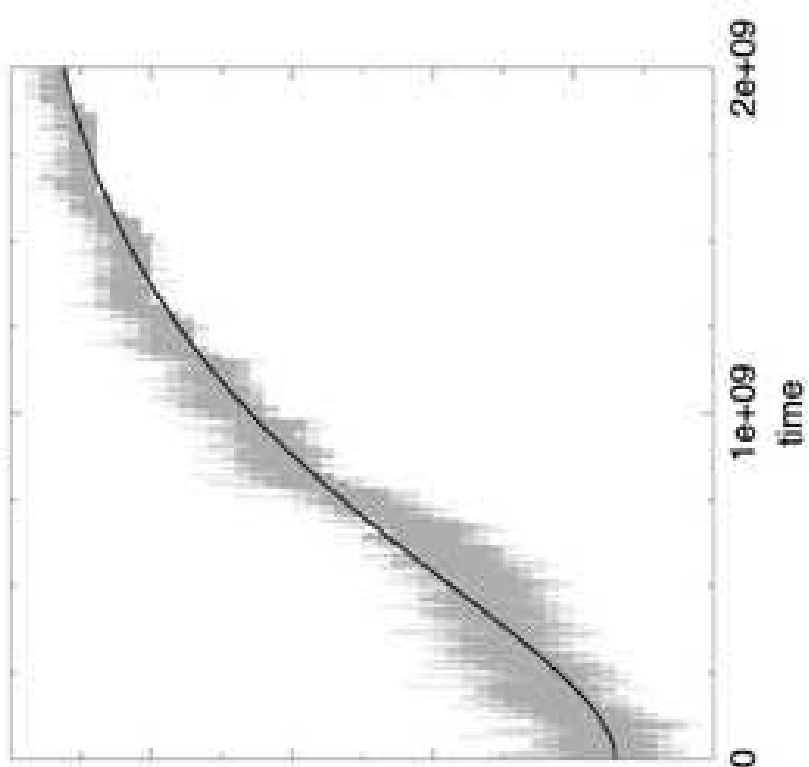




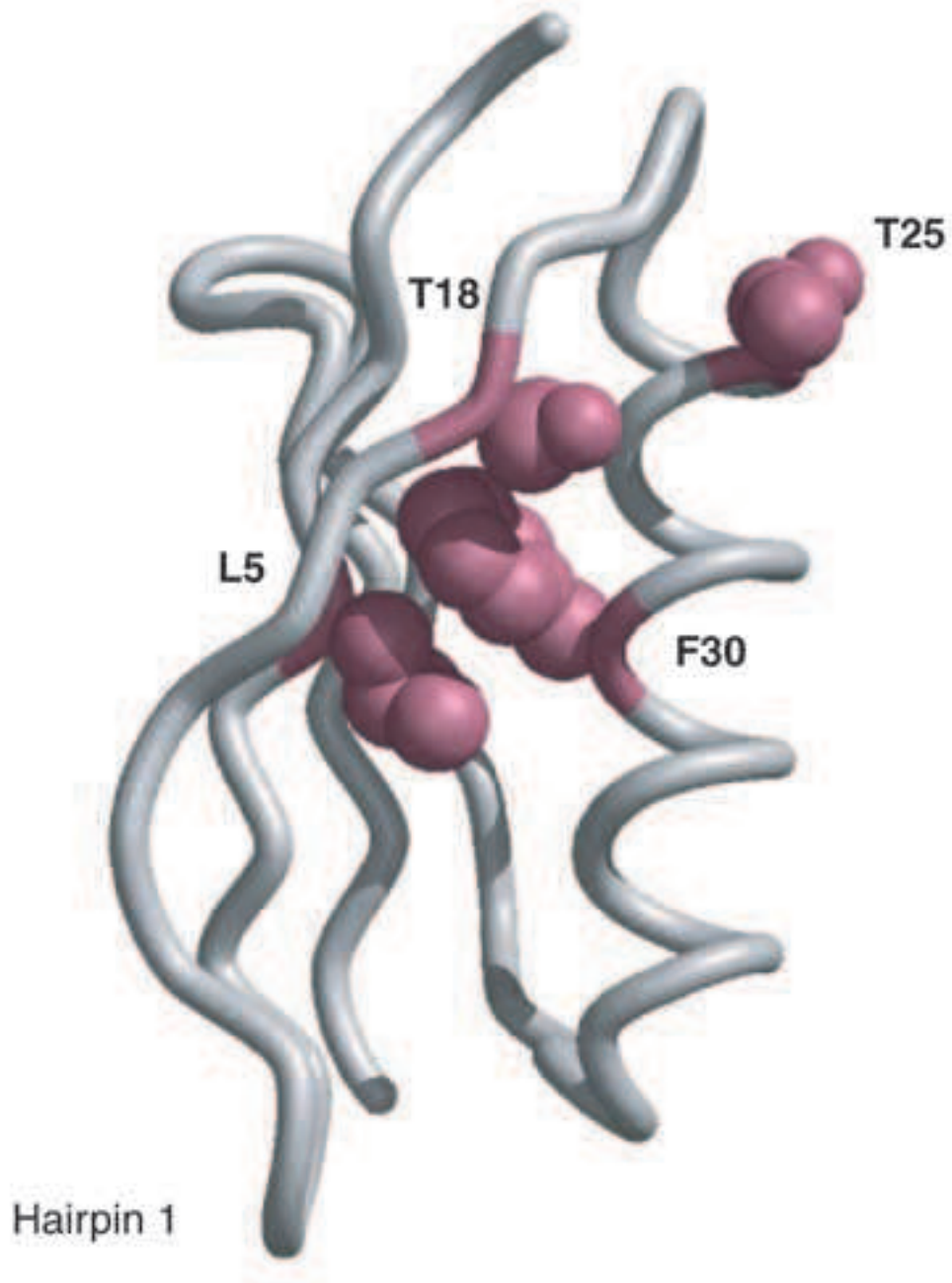
Phenylalanine 30



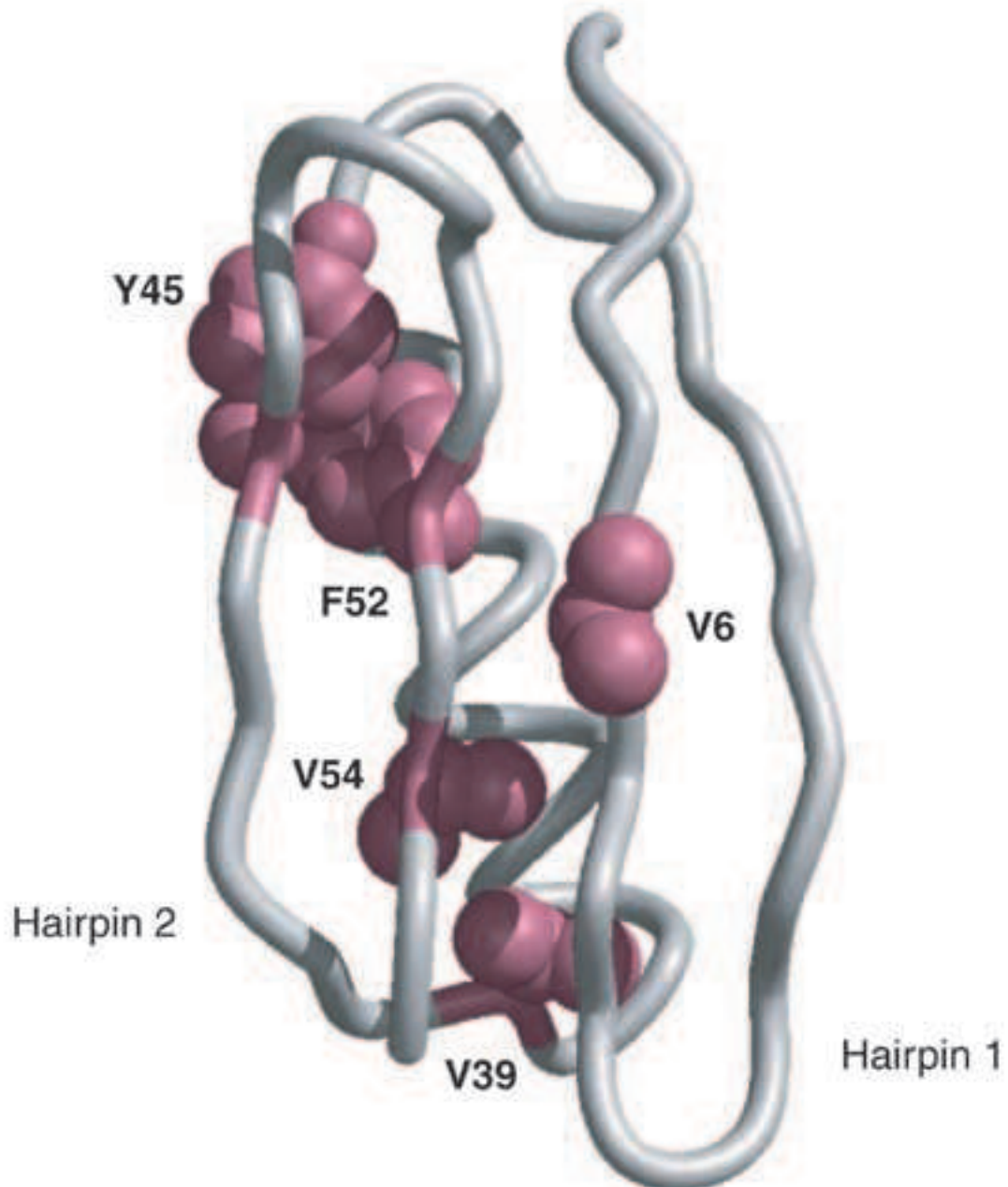
Phenylalanine 52



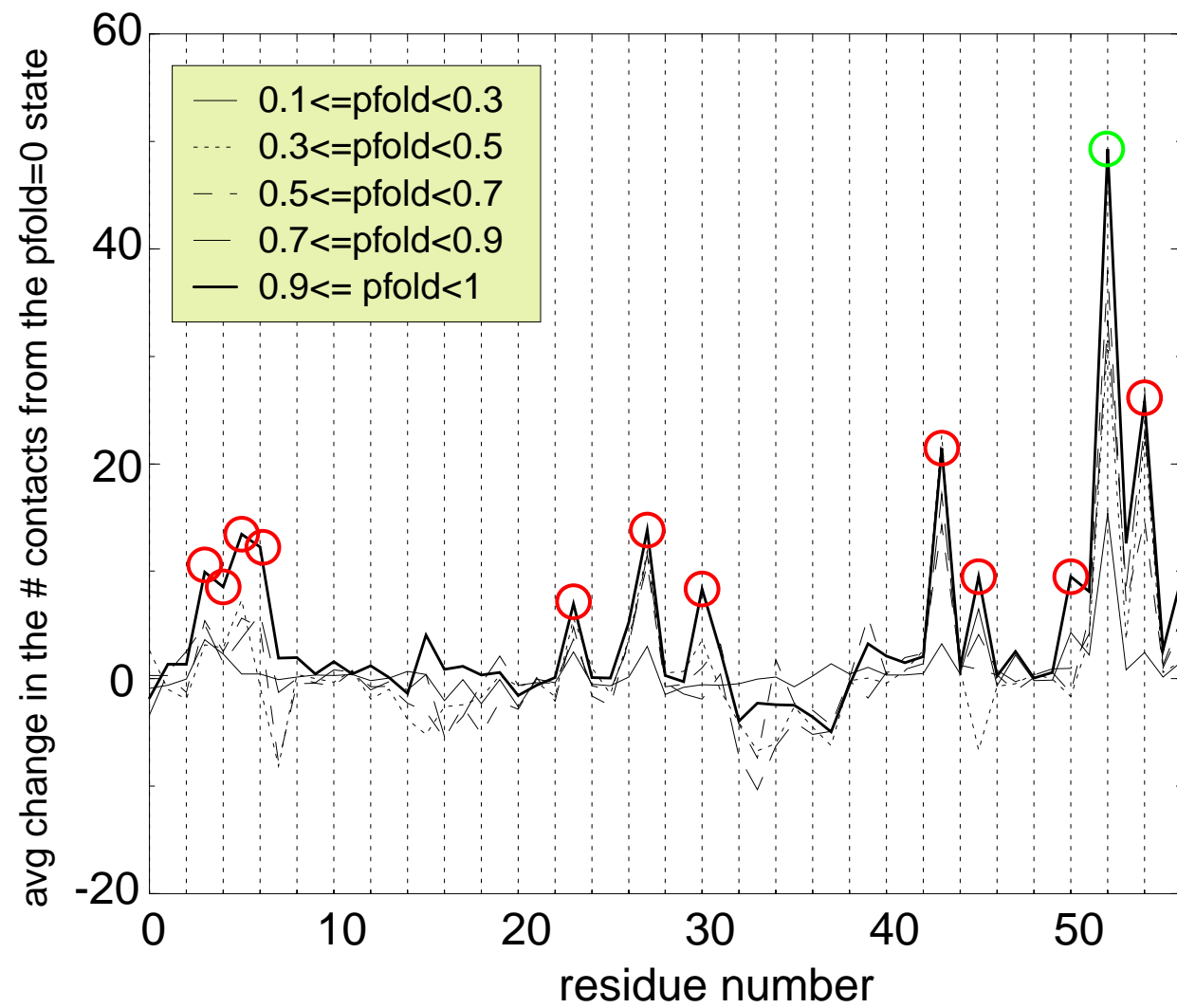
Protein G:  
Fast residues, pre-intermediate

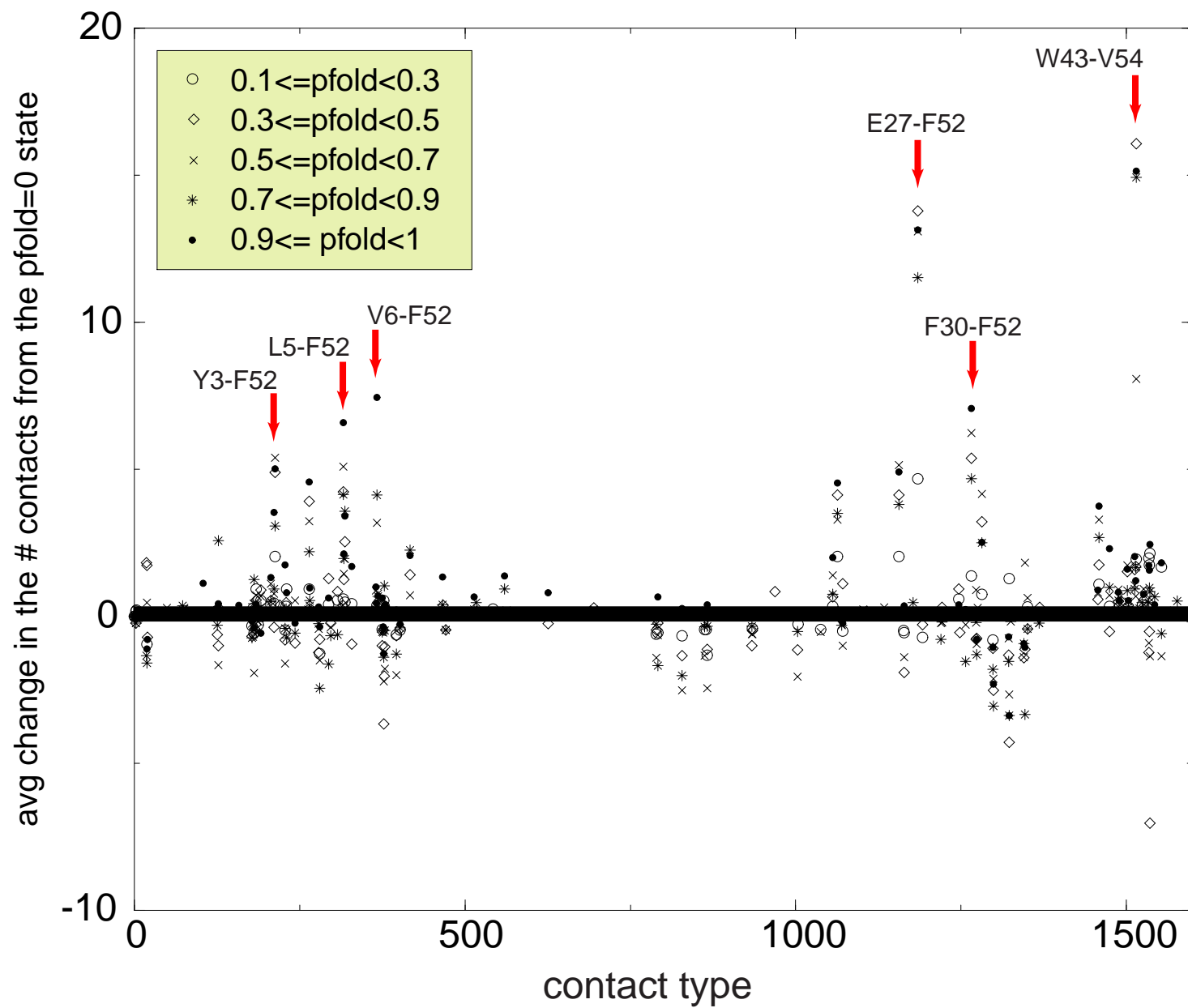


Protein G:  
Fast residues, post-intermediate

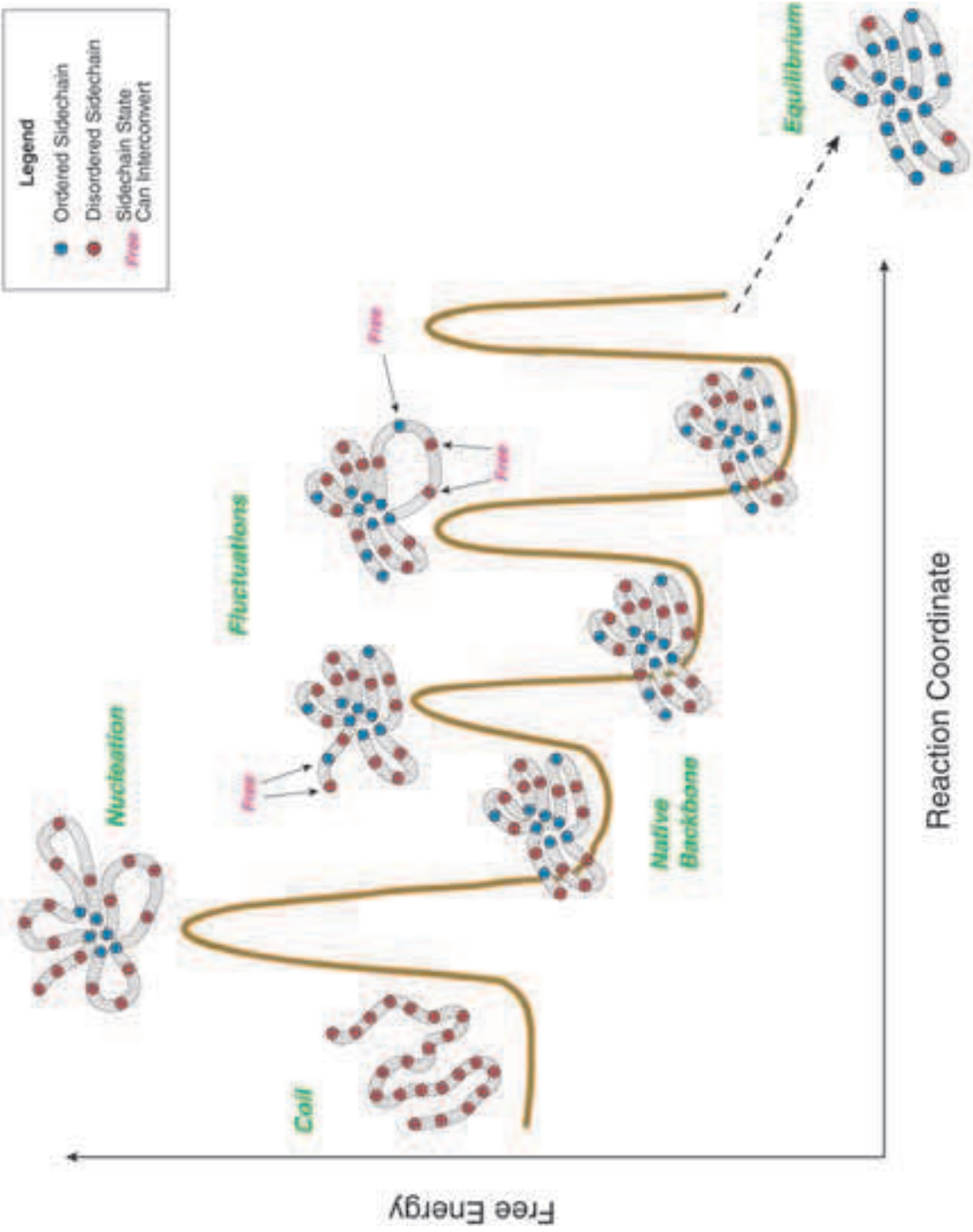








- Legend**
- Ordered Sidechain
  - Disordered Sidechain
  - Sidechain State
  - Free Can Interconvert



Reaction Coordinate

Free Energy

Fluctuations

Nucleation

Coil

Native Backbone

Equilibrium

Figure 1:

Figure 2:

Figure 3:

Figure 4:

Figure 5:

Figure 6:

Figure 7:

Figure 8:

Figure 9:

Figure 10:

Figure 11:

Figure 12:

Figure 13: